



OAK RIDGE NATIONAL LABORATORY LIBRARIES



3 4456 0539372 1

ORNL/SUB-33200/1

*cy. 3*

FUSION ENERGY DIVISION LIBRARY

# DEVELOPMENT PROGRAM FOR A 200 kW, CW, 110 GHz GYROTRON

FED LIBRARY LTR 1980

## QUARTERLY REPORT NO. 1 JUNE THROUGH SEPTEMBER 1979

Contract No. W-7405-ENG-26

Prepared by

HUGHES AIRCRAFT COMPANY  
Electron Dynamics Division  
3100 West Lomita Boulevard  
Torrance, California 90509

for  
OAK RIDGE NATIONAL LABORATORY  
Oak Ridge, Tennessee 37830  
operated by  
UNION CARBIDE CORPORATION  
for the  
DEPARTMENT OF ENERGY

This report was prepared as an account of work sponsored by an agency of the United States Government. Neither the United States Government nor any agency thereof, nor any of their employees, contractors, subcontractors, or their employees, makes any warranty, express or implied, nor assumes any legal liability or responsibility for any third party's use or the results of such use of any information, apparatus, product or process disclosed in this report, nor represents that its use by such third party would not infringe privately owned rights.

# **DEVELOPMENT PROGRAM FOR A 200 kW, CW, 110 GHz GYROTRON**

K. W. Arnold, J. J. Tancredi, M. Caplan, K. W. Ha,  
D. N. Birnbaum, W. Weiss

## **QUARTERLY REPORT NO. 1 JUNE THROUGH SEPTEMBER 1979**

Contract No. W-7405-ENG-26

Prepared by

HUGHES AIRCRAFT COMPANY  
Electron Dynamics Division  
3100 West Lomita Boulevard  
Torrance, California 90509

for  
OAK RIDGE NATIONAL LABORATORY  
Oak Ridge, Tennessee 37830  
operated by  
UNION CARBIDE CORPORATION  
for the  
DEPARTMENT OF ENERGY

## TABLE OF CONTENTS

<u>Section</u>		<u>Page</u>
I.	INTRODUCTION	1-1
II.	BACKGROUND	2-1
	2.1 Introduction	2-1
	2.2 Cavity Design	2-8
	2.3 Design Approach	2-26
III.	PROGRESS	3-1
	3.1 General	3-1
	3.2 RF Circuit	3-1
	3.3 Electron Gun	3-8
	3.4 Collector	3-28
	3.5 Solenoid	3-31
	3.6 Power Supply	3-32
	3.7 Beam Analyzer/Tester	3-34
	3.8 Test Equipment	3-38
IV.	PROGRAM SCHEDULE AND PLANS	4-1

## LIST OF ILLUSTRATIONS

<u>Figure</u>	<u>Page</u>
1-1	1-3
2-1	2-2
2.2-1	2-10
2.2-2	2-13
2.2-3	2-17
2.2-4	2-18
2.3-1	2-28
2.3-2	2-29
2.3-3	2-31
3.2-1	3-3
3.2-2	3-4
3.2-3	3-6
3.2-4	3-7

LIST OF ILLUSTRATIONS (CONTINUED)

<u>Figure</u>		<u>Page</u>
3.2-5	Scale drawing of beam-cavity geometry for a first order design using a cylindrical cavity.	3-9
3.3-1	Emission ratio vs cathode angle.	3-11
3.3-2	Sample computer print-out from parametric study.	3-13
3.3-3	Conventional magnetron injection gun (A thru F).	3-15
3.3-4	Modified magnetron injection gun (A thru G).	3-21
3.4-1	Schematic of waveguide and electron collector.	3-29
3.4-2	Electron extraction between facing parabolic antenna proposed by R. Randl of Oak Ridge.	3-30
3.7-1	Proposed method of measuring axial velocity spread.	3-36
4-1	Work breakdown structure for 110 GHz Gyrotron - Union Carbide Corporation.	4-4
4-2	Milestone schedule.	4-5

## I. INTRODUCTION

The objective of this program is the design and development of a millimeter-wave device to produce 200 kw of continuous-wave power at 110 GHz. The device, which will be a gyrotron oscillator, will be compatible with power delivery to an electron-cyclotron plasma. Smooth control of rf power output over a 17 dB range is required, and the device should be capable of operation into a severe time-varying rf load mismatch.

The technical baselines for the gyrotron and the associated power supply are shown in Table I. In the gyrotron, which is shown schematically in Figure 1-1, the electrons are formed into a hollow beam by a magnetron-injection electron gun with a considerable amount of their energy in rotation. A gradually rising magnetic field compresses the beam in diameter and at the same time increases the orbital energy according to the theory of adiabatic invariants until approximately 2/3 of the beam energy is in rotation and the rotational frequency is 110 GHz; at this point the magnetic field becomes uniform and the beam enters a quasi-optical open cavity where the spinning electrons interact with the eigenmode of the cavity. The rf energy builds up at the expense of the rotational energy of the dc beam. The spent beam enters the region of decreasing magnetic field, undergoes decompression and impinges on the collector. The latter also functions as the output waveguide. In order to handle the power in the spent beam and the power dissipation in the window the output waveguide tapers up from the cavity diameter to an appropriate value.

The duration of the program is 36 months, to encompass the building and test of up to twelve devices in addition to a beam analyzer and beam tester. The program is planned for dual approaches to the electron gun and collector. The magnetron injection gun is well understood and allows the use of the extraction anode (as well as cathode temperature variation)

TABLE I

<u>The Gyrotron</u>	
Frequency	110 GHz
Power out	200 kW RF
Electronic efficiency	35%
Beam voltage	70 kV
Beam current	8.2 A
Magnetic field	42.46 kg
Transverse to longitudinal velocity ratio	1.5
Cathode Loading	8 A/cm <sup>2</sup>
Cathode radius	0.44 cm
Cathode length	0.36 cm
<u>The Power Supply</u>	
Voltage rating	100 kV dc
Current rating	10 A
Anode supply voltage	0-35 kV dc
Anode supply current	200 mA
Heater supply voltage	0-15 V, ac
Heater supply current	15 A
Operating Modes:	
1.	10 $\mu$ s pulse length
2.	1 ms - 10 s pulse length
3	cw

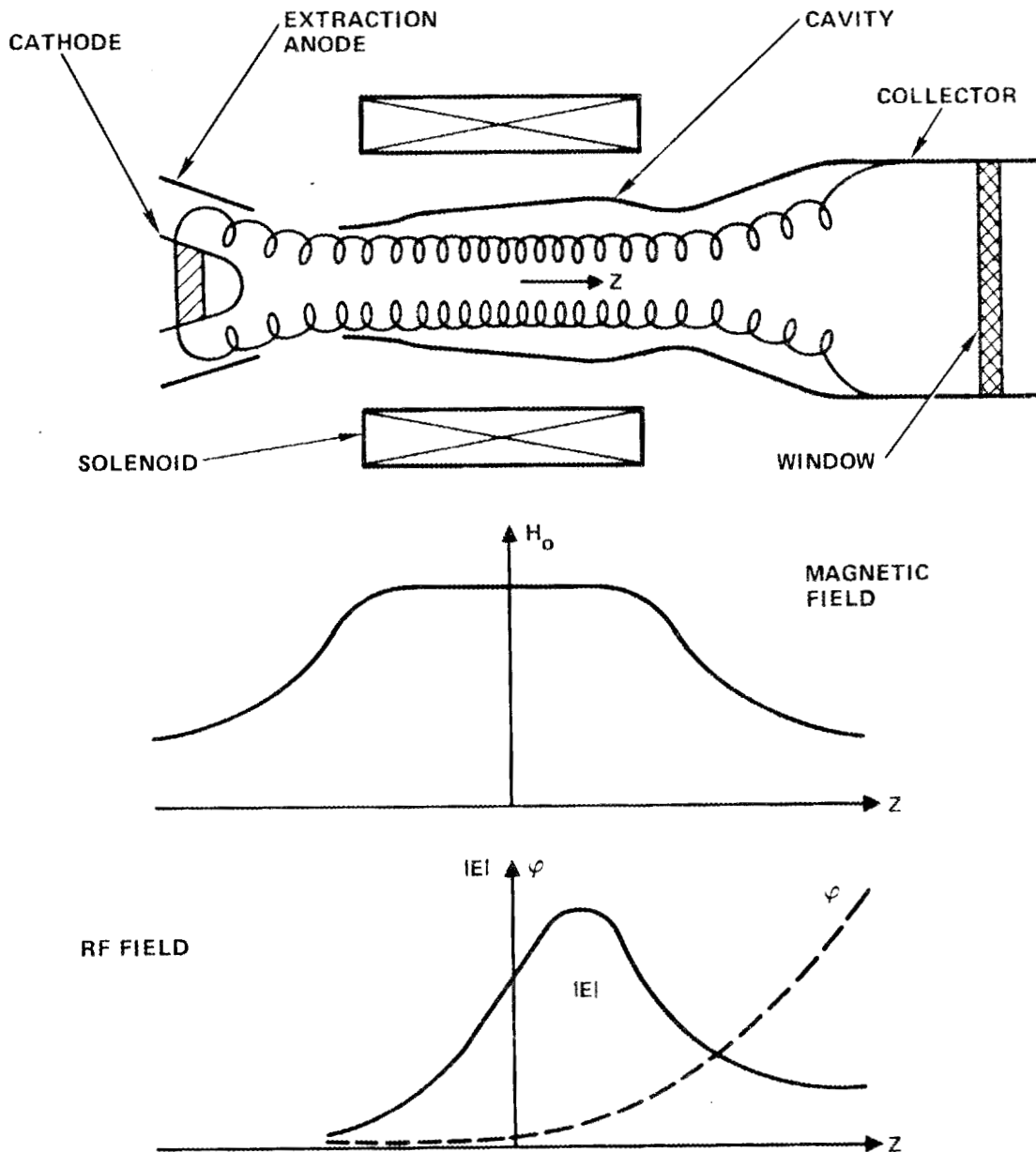


Figure 1-1 Schematic of gyrotron oscillator showing applied magnetic field and the rf field and gain in the cavity.

to vary the rf power out. The diode gun configuration, however, could lead to lower thermal spread in the electron beam, and thus to a higher efficiency. It also has a somewhat simpler mechanical construction. For rapid variation of the rf power out, the diode gun could be designed with a control electrode, in the form of an aperture grid or a modulated anode. Similarly, at least two design approaches will be taken with respect to the collector, which has to be able to dissipate over 550 kw in under-pressed operation. Fabrication and processing of prototype devices will proceed in parallel.

During this first reporting period work has begun on a number of design tasks, including the magnetron injection gun, rf circuit, collector and power supply specifications. These activities are detailed in Section III of this report, following the delineation of relevant background material.

## II. BACKGROUND

### 2.1 INTRODUCTION

During the past decade, the available power levels at millimeter wavelengths have increased dramatically. Hughes has achieved 5 to 7 kW at 55 GHz and 1 kW cw at 94 GHz from coupled-cavity TWT amplifiers. These results define the current state of the art for cw devices that rely on slow-wave interaction circuits. This is illustrated by the solid curves shown in Figure 2-1.

Although the TWT has been in the forefront as a millimeter-wave high-power source, it has become increasingly evident that fundamental limitations to the TWT approach will allow only relatively small further increases in performance. These limitations include voltage breakdown, thermal dissipation and lower efficiency.

As illustrated in Figure 2-1, other standard amplification devices (such as klystrons and crossed-field amplifiers) have not shown the same potential for high-power performance in the millimeter-wave region as the coupled-cavity TWTs. For klystrons, the limitations arise from the problems associated with large power levels in a single, relatively high-Q cavity. For crossed-field devices, the fact that the electron beam is collected on the delicate rf interaction circuit prevents a high-average-power capability.

The average power performance for devices of this type drops below about 100 W at 50 GHz. The only method known for increasing the power of these devices is to extend the interaction circuit (or cavity) in a direction transverse to the beam, thereby distributing the losses over a larger area. For example, a multiple-beam klystron, which effectively accumulates the power from up to 40 klystrons into one rf circuit, has been demonstrated.<sup>1</sup> More than an order-of-magnitude increase in average

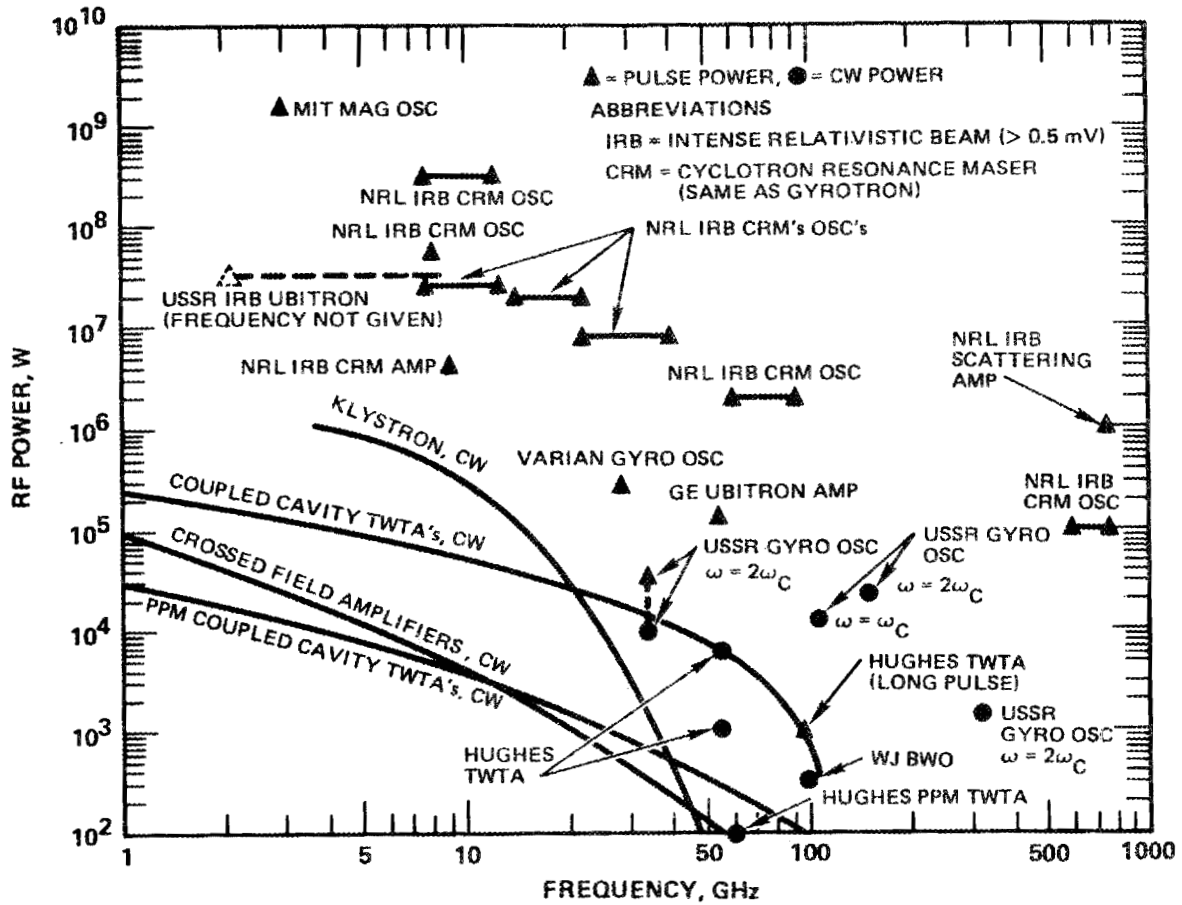


Figure 2-1 Plots of power versus frequency for high-power devices in the microwave and millimeter wave regimes. (Dots are CW power, triangles are pulsed power.)

power is thus possible, but the complexity is increased greatly and the resulting circuits require mode control to prevent undesirable oscillations.

Studies to date indicate that so-called fast-wave, or periodic beam, devices are achieving a breakthrough in power generation for millimeter-wave applications. These devices use a periodic electron beam to interact with a fast wave in a relatively large low-loss waveguide, thus circumventing the power-handling limitations of slow-wave circuits. Although these devices sometimes require higher beam voltages and operate in an overmoded condition, they offer enormously improved thermal dissipation and power-handling capabilities in return.

One such fast-wave device, the Ubitron, was pursued actively in the late 1950s and early 1960s, with much of the work done by General Electric.<sup>2-4</sup> At that time, the device was proven experimentally, but applications and support for high-power millimeter-wave tubes were lacking and the development effort was terminated. GE's Ubitron achieved 150 kW of peak power with about 6% efficiency at 54 GHz (Ref 5 and Figure 2-1).

For the proposed application, the Ubitron is not an attractive approach. The efficiency of 6% is significantly lower than that of a gyrotron device and the construction and cooling of the RF circuit is much more complicated. PPM focusing was found to be unsuitable for cylindrical Ubitron devices as this type of focusing system inherently scallops the beam. Because the rf gain mechanism depends strongly on the radial position of the beam, the scalloping motion is prohibitive.<sup>6</sup>

Other fast-wave devices have been reported in the literature,<sup>7-9</sup> the most important of which is the gyrotron<sup>10-14</sup> (or cyclotron resonance maser, CRM). The Naval Research Laboratory (NRL) has done extensive research on this device using an intense relativistic beam.<sup>15-18</sup> Megawatt levels of pulsed power have been reported at frequencies up to

90 GHz (see Figure 2-1). NRL's theoretical work has provided the basis for rf design of gyro-devices.

Most gyrotron applications research has been done in the USSR, where work on these devices has apparently been going on for a decade. Although the principles of gyro-TWA amplifiers have been described by Soviet authors,<sup>10,11</sup> single-cavity oscillators are the only high-power operating devices known to have been reported in the literature. The highest average power levels were 12 kW at 107 GHz and 1 kW at 350 GHz. The efficiencies of these two gyrotrons were 30% and 6%, respectively, with the latter device operating at the second harmonic of the cyclotron frequency. Electronic efficiencies up to 43% have been reported. Beam voltages range from 19 to 27 kV.

Jory et al.<sup>19</sup> reported on gyro-klystron development at 28 GHz in the USA. Pulsed power outputs of up to 248 kW at 34% efficiency have been obtained from a single-cavity oscillator. This result is plotted in Figure 2-1. Also, 40-dB gain was reported in a three-cavity gyro-klystron amplifier with 50-kW pulse output at 7% efficiency.

Based on these results and large signal performance predictions of a preliminary design, the successful development of a 200 kW, cw gyrotron at 110 GHz appears achievable, although the very high average power densities required on the device do represent a considerable technical challenge. An oscillator is preferred over an amplifier for a number of reasons, chief among them being the elimination of the need for an rf source as well as an input coupler, and the greater likelihood of stable operation.

REFERENCES FOR SECTION 2-1

1. M. R. Boyd, "The Multiple-Beam Klystron," Trans. IRE ED-9, 247, May 1962.
2. R. M. Phillips, "The Ubitron - a High Power Traveling Wave Tube Based on Periodic Beam Interaction in an Unloaded Waveguide," IRE ED-7, 231-241, October 1960.
3. L. C. Bacon, E.E. Enderby, and R. M. Phillips, "V-Band Ubitron Amplifier Development," prepared by G.E. Company under Contract AF 33(616)-8356, April 1962.
4. C. E. Enderby and R. M. Phillips, "V-Band Ubitron Amplifier Development," Tech Documentary Report No. ASD-TDR-63-847, Jan. 1964, prepared for AF Avionics Lab, by G. E. TWT Product Section, under Contract AF 33(616)-8356.
5. C. E. Enderby and R. M. Phillips, "The Ubitron Amplifier - A High-Power Millimeter-Wave TWT," Proc. IEEE 53, 1648, October 1965.
6. J. M. Baird, S. Sensiper, K. Amboss, and J. F. Henry, "Millimeter Wave Ubitron Development," Hughes Research Laboratories, Technical Report, Contract F30602-76-C-0215, February 1977.
7. R. H. Pantell, Proc. of Symp. on Millimeter Waves, N.Y. (1959), p. 301; Proc. IRE 47, No. 6, 1146 (1959).
8. K. I. Talbot, "Rotating Beam Devices," Microwave Device and Physical Electronics Laboratory Electrical Engineering Dept., Technical Report Nos. MDL-Q21 through MDL-Q24 (1967 and 1968).

9. R.L. Schreiver and C. C. Johnson, "Rotating Beam Devices," Quarterly Report, December 21, 1966, Technical Report MDL-Q19; Microwave Device and Physical Electronics Laboratory, University of Utah, Contracts NonR1288(05) and AF33(615)3686.
10. V. A. Flyagin, A. V. Gaponov, M. I. Petelin, V. K. Yulpatov, "The Gyrotron." To be published. (A copy of this paper was obtained through through provate communication with NRL.)
11. A. V. Gaponev, A. L. Goldenberg, M. I. Petelin, V. K. Yulpatov, Copyright No. 223931 with priority of 24 March 1967, Official Bulletin KDIO of SM USSR, No. 11, 200 (1976).
12. N. I. Zaytsev, F. B. Pankratove, M. I. Petelin, and V. A. Flyagin, "Millimeter and Submillimeter Waveband Gyrotrons," Radiotekhnika i elektronika, 1056-1060 (1974).
13. D. V. Kisel, G. S. Korablev, V. G. Navel'yev, M. I. Petelin, and SH. YE. Tsimring, "An Experimental Study of a Gyrotron Operating at the Second Harmonic of the Cyclotron Frequency with Optimized Distribution of the High-Frequency Field" (1973).
14. S. I. Kremontsov, M. D. Reiser, and A. V. Smorgonskii, "Ubitron - The Oscillator with a Relativistic Electron Beam," Pis'ma v. Zhurnal Tekhn. Fiziki 2, 453-457, May 26, 1976.
15. M. Friedman, M. Herndon, Phys. Rev. Lett. 17, No. 4, 210 (1972).
16. V. I. Granatstein, P. Sprangle, R. K. Parker, and M. Herndon, "An Electron Synchrotron Maser Based on an Intense Relativistic Electron Beam," J. Appl. Phys. 46, p. 2021, May 1975.

17. V. L. Granastein, P. Sprangle, M. Herndon, R. K. Parker, and S. P. Schlesinger, "Microwave Amplification with an Intense Relativistic Electron Beam," J. Appl. Phys. 46, 3800, Sept. 1975.
18. V. L. Granatstein, M. Herndon, P. Sprangel, J. Carmel, and J. Nation, Plasma Phys. 1, No. 1, 23 (1975).
19. H. R. Jory, et al., "Gyrotrons for High Power Millimeter Wave Generation," Proc. International Electron Devices Meeting, Washington, D.C., Dec. 5-7, 1977, p. 234.

## 2.2 CAVITY DESIGN

With a well designed cavity<sup>1</sup> the gyrotron converts a large fraction of the rotational energy of the dc beam into rf with an overall electronic efficiency of about 35%. Hence the required beam power for 200 kW of output power is about 570 kW. The efficiency has a broad maximum<sup>2</sup> at a value of  $\gamma \approx 1.10$ , i.e., at about 70 kV. This voltage is also acceptable from an electron optical point of view since the corresponding beam current of 8.15 Amps can be drawn from a cathode of moderate size with an emission density which is achievable with impregnated tungsten matrix materials. Voltage breakdown in the gun and in the power supply does not present a major design problem. The magnetic field in the cavity is determined only by the operating frequency and for 110 GHz amounts to 42.46 kG. A field of this magnitude must be generated by a superconducting magnet. Higher harmonic operation with a field of one quarter this value may have allowed the use of a water cooled magnet; however the attendant loss of efficiency produces problems in other areas and makes this mode of operation unattractive.

The efficiency of operation is predicated on a low axial beam velocity spread and the latter is a sensitive function of the extraction anode voltage.<sup>3</sup> It appears possible therefore to tailor the microwave power pulse rise time by spoiling the efficiency of the device by changing the extraction anode voltage. Preliminary design parameters are given in Table 2.2-1.

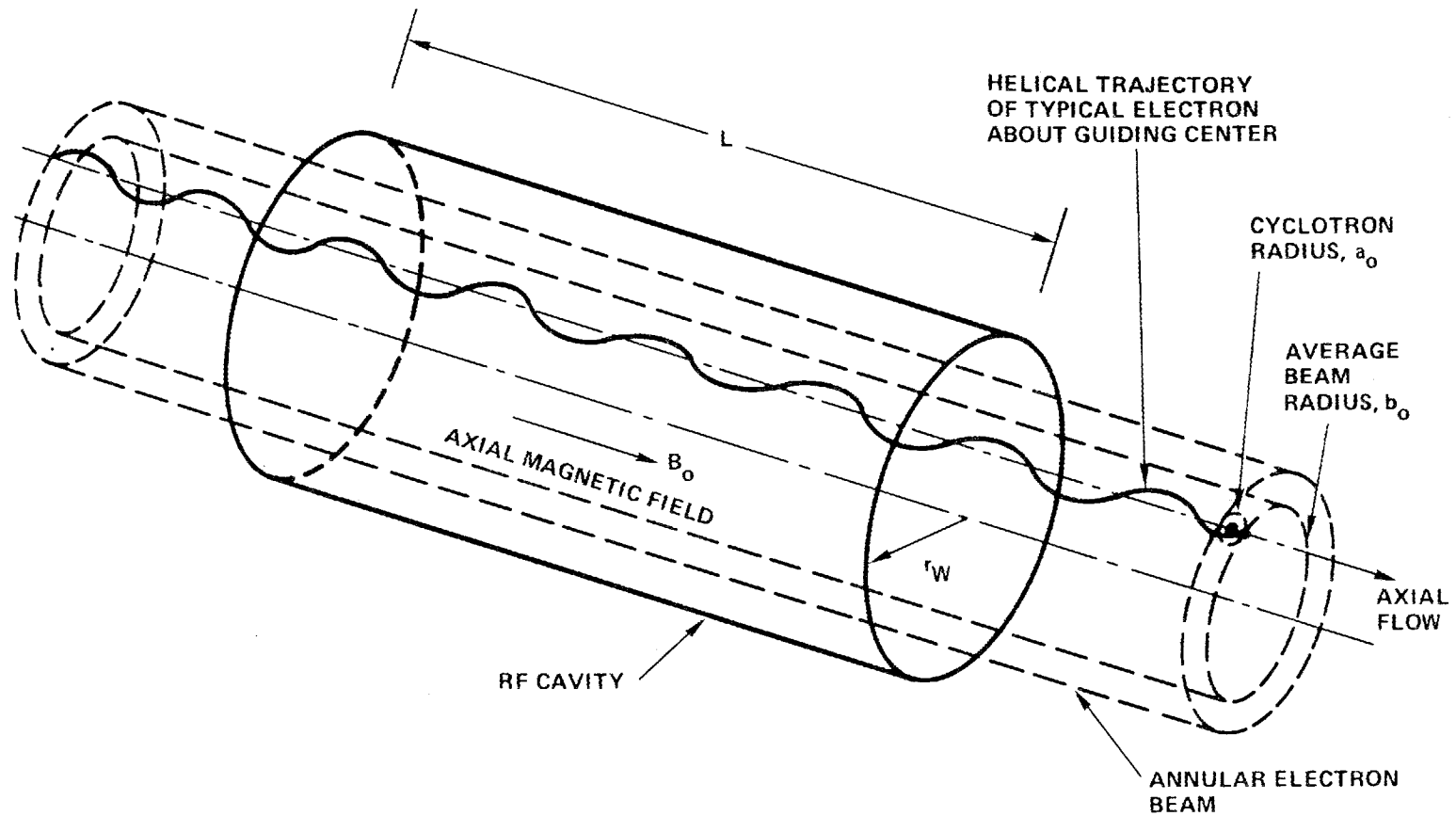
The small signal theory of the RF cavity interactions in a gyro-magnetron is treated in detail by Chu.<sup>4</sup> The geometric model for the analysis is shown in Figure 2.2-1; a definition of the variables used in this report appears in Table 2.2-2.

TABLE 2.2-1  
PARAMETERS OF THE GYROTRON

Beam voltage	$\phi_B$	70 kV
Beam current	I	8.2 amp
Magnetic field	$B_o$	42.46 kG
Transverse/longitudinal velocity ratio	$\alpha$	1.5
Relativistic gamma	$\gamma$	1.1370
Beam velocity*	$v/c$	0.4759
Axial velocity*	$v_z/c$	0.2640
Rotational velocity*	$v_{\pm}/c$	0.3960
Cathode loading	$j_c$	8.0 A/cm <sup>2</sup>
Cathode radius	$r_c$	0.44 cm
Cathode length	$\ell$	0.36 cm
Mean radius of beam in cavity	$b_o$	0.08 cm
Larmor radius	$a_o$	0.018 cm
Cavity diameter (nominal)	d	0.611 cm
Length of cavity (nominal)	L	1.833 cm
Diameter of output waveguide	$d_w$	1.23 cm
Electronic efficiency <sup>1</sup>	$\eta$	35%
Cavity Q		232
RF power	$P_o$	200 kW
Frequency	f	110 GHz

\*Normalized to c, velocity of light

<sup>1</sup>With cavity tapering



2-10

Figure 2.2-1 Diagram showing geometric relationships of beam in RF cavity in gyro-klystron.

TABLE 2.2-2

Description	Symbol and Defining Equation
Speed of light	c
Electron charge, rest mass	e, m <sub>0</sub>
Beam voltage, current	V <sub>0</sub> , I <sub>0</sub>
Power output, Beam power	P <sub>0</sub> · P <sub>b</sub>
Electronic efficiency	η
Axial magnetic field	B <sub>0</sub>
Average beam radius	b <sub>0</sub>
Larmor radius of electrons	a <sub>0</sub>
Radius of cavity wall	r <sub>w</sub>
Number of electrons per unit length	N
Cyclotron frequency harmonics mode	s
Indices for radial, longitudinal modes	n, ℓ
Relativistic correction factor	$\gamma_0 = 1 + (e/m_0 c^2) V_0 = 1 - (v_0/c)^2^{-1/2}$
Relativistic cyclotron frequency	$\omega_0/\gamma_0 =  e/m B_0/\gamma_0$
Space charge parameter	$v = N e^2/m_0 c^2$
Cavity length and normal form	L, $\bar{L} = L/r_w$
Total electron velocity	$v_0 = \sqrt{1 - 1/\gamma_0^2}$
Transverse electron velocity	$v_{\pm 0} \left\{ \begin{array}{l} v_{\perp 0}^2 + v_{z0}^2 = v_0^2 \\ v_{z0} \end{array} \right.$
Longitudinal electron velocity	$v_{z0}$
Normalized velocities	$(\beta_0, \beta_{\perp}, \beta_z) = (v_0, v_{\perp 0}, v_{z0})/c$
Frequency, radian frequency	f, $\omega \equiv 2\pi f$
Normalized radian frequency	$\bar{\omega} \equiv \omega r_w / c$
Transverse propagation constant	$k_n = \chi_n / r_w$
nth nonzero root of J <sub>1</sub> (χ)	χ <sub>n</sub>
Longitudinal propagation constant	k <sub>z</sub> = πℓ/L
Normalized propagation constants	$k_n \equiv k_n r_w = \chi_n, \bar{k}_z = k_z r_w$
Cavity transit time	τ = L/v <sub>z0</sub>
Normalized transit time	$\bar{\tau} = \tau c / r_w$
Forward wave transit angle	Δ = (ω - k <sub>z</sub> v <sub>z0</sub> - sΩ <sub>0</sub> /γ <sub>0</sub> ) τ
Backward wave transit angle	Δ' = (ω + k <sub>z</sub> v <sub>z0</sub> - sΩ <sub>0</sub> /γ <sub>0</sub> ) τ
Total field energy in cavity	W <sub>f</sub>
Cavity Q	Q = ωW <sub>f</sub> /P <sub>0</sub>
Peak cavity electric field	E <sub>00</sub>
Beam energy gain per transit	F

It is assumed in this analysis that all of the electrons entering the cavity have the total energy and a fixed ratio of transverse-to-longitudinal velocity (i.e., no velocity spread;  $\alpha \equiv v/v_z = \text{constant}$ ). It is also assumed that the guiding centers of all electrons have the same radius,  $b_o$ , giving an annular beam thickness is twice the cyclotron radius,  $a_o$ .

Assuming that the RF energy is reflected at the ends of the cavity the electromagnetic fields for the  $TE_{onl}$  modes in the cavity are given by

$$E_{\theta} = E_{\theta o} J_1(k_n r) \sin(k_z z) \cos(\omega t) \quad (2.2-1)$$

$$B_r = \left(\frac{k_z}{\omega}\right) E_{\theta o} J_1(k_n r) \cos(k_z z) \sin(\omega t) \quad (2.2-2)$$

$$B_z = -\left(\frac{k_n}{\omega}\right) E_{\theta o} J_0(k_n r) \sin(k_z z) \sin(\omega t) \quad (2.2-3)$$

For operation at the fundamental cyclotron frequency ( $s = 1$ ) the electron beam-RF interaction is optimized by making the average beam radius  $b_o$  correspond to a peak in the electric field  $E_{\theta}$ . For the  $n = 2$  modes, this beam radius is  $b_o = 0.26 r_w$ .

The frequency of the cavity eigen modes of oscillation is given by

$$\omega_{nl} = c \left(k_z^2 + k_n^2\right)^{1/2} \quad (2.2-4)$$

which can be plotted as a set of points along the dispersion curve, for cylindrical waveguide having the same radius,  $r_w$ . An example of such a diagram is shown in Figure 2.2-2. In this figure we have also plotted the  $s$ th beam cyclotron mode in such a way that it passes through the  $TE_{Onl}$  cavity mode.

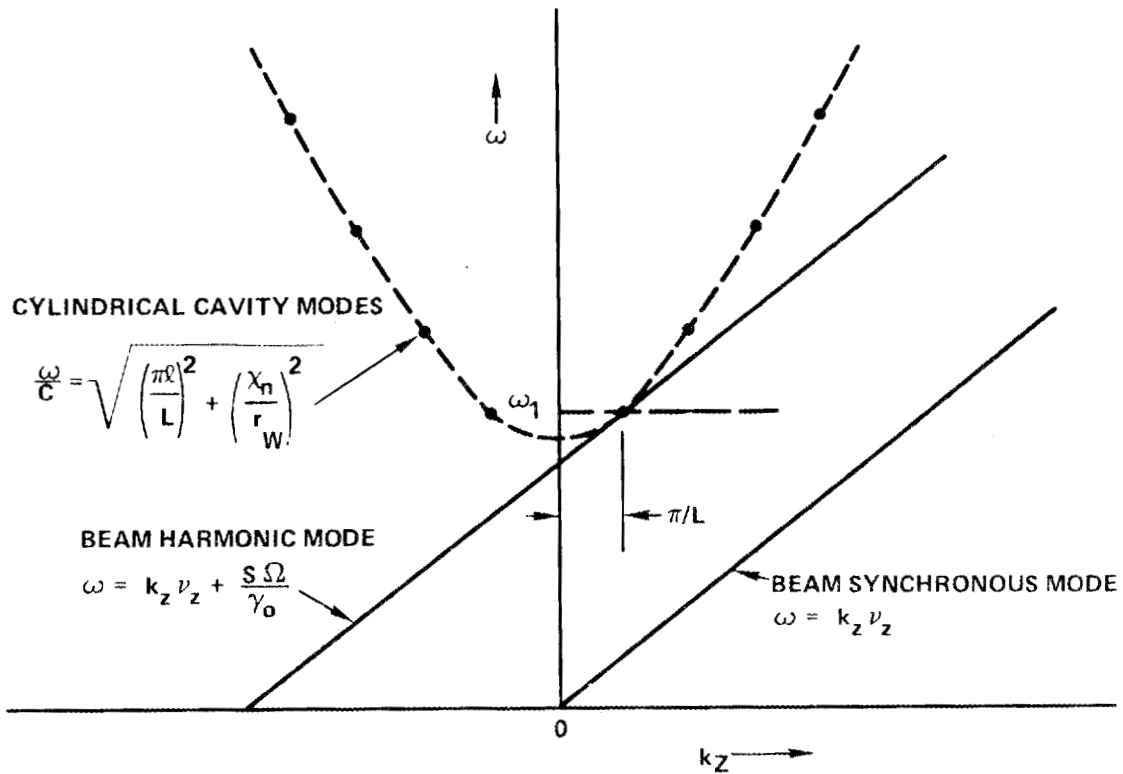


Figure 2.2-2 Conceptual dispersion diagram showing the beam and cavity modes in a configuration which will excite the  $TE_{011}$  cavity mode at the  $s$ th beam harmonic.

The Q of a cavity is defined as the ratio of energy stored,  $W_f$ , to the energy lost per radian,  $P_L / \omega$

$$Q = \frac{W_f}{\left(\frac{P_L}{\omega}\right)} \quad (2.2-5)$$

For a gyro monotron, the power loss  $P_L$  is made up of the power dissipated in the walls of the cavity,  $P_D$ , plus the output Power,  $P_o$ , coupled to the output wave guide.

$$P_L = P_D + P_o$$

For most practical cases  $P_o \gg P_D$  and therefore the loaded Q is determined essentially by  $P_o$ .

The stored energy in the cavity is determined for each mode by integrating the energy density ( $\epsilon E^2 + \mu H^2$ ) for that mode over the volume of the cavity. Since the field shape is fixed for each eigen mode of the cavity, this procedure results in

$$W_{fm} = \xi_m E_{\theta o}^2 \quad (2.2-6)$$

where  $\xi_m$  is the cavity "form factor" for the mth eigen mode and  $E_o$  is the peak transverse electric field. Using Equations 2.2-1, 2.2-2 and 2.2-3, for example, the stored energy for the cylindrical cavity is given by

$$W_{fn} = \frac{\pi c L}{4} r_w^2 J_o^2 (\chi_n) E_{\theta o}^2 \quad (2.2-7)$$

The value of the cavity Q is a key factor in the design of gyromonotrons. In the small signal case, the threshold beam power required to start

oscillations is inversely proportional to the cavity Q. In the large signal case, saturated output power occurs at a specified value of peak electric field which determines (in conjunction with the output power and the cavity form factor) the design value of the cavity Q. Thus, in operation the cavity Q determines both the starting beam power and the saturated output power. For this reason, it is important that the cavity Q determined in the RF design be achieved as nearly as possible in the physical construction.

The losses in the cavity can be estimated by comparing the loaded and unloaded Q's of the cavity. As previously noted the loaded Q is given by

$$Q_L = \frac{\omega W_f}{P_D + P_o} \approx \frac{\omega W_f}{P_o} \quad (2.2-8)$$

and the unloaded Q by

$$Q_u = \frac{\omega W_f}{P_D} \quad (2.2-9)$$

Since the condition of interest is to determine  $P_D$  when  $P_o$  is 200 kW,  $W_f$  is approximately the same in both equations and can be eliminated to give

$$P_D \approx \left( \frac{Q_L}{Q_u} \right) P_o$$

The theoretical unloaded Q of a TE<sub>021</sub> circular cavity can be calculated from well known equations.<sup>5</sup> For a copper cavity ( $c = 4(10^7)$  mhos/m) with a length to diameter ratio of 6,  $Q_u = 12200$  at 110 GHz. Anticipating a loaded Q of approximately 230 then gives

$$\frac{P_D}{P_o} \approx 1.9\%$$

For the power level of the proposed device, the dissipated power in the cavity is about 3.8 kW.

The power dissipated through waveguide losses is another factor which is easily calculated from well established theory.<sup>6</sup> Figure 2.2-3 gives the dissipated power per cm in a circular waveguide carrying 200 kw of power in the TE<sub>02</sub> mode (copper assumed).

Another important cavity design consideration for gyro-monotrons is the cavity shape (form factor). By selecting a cavity shape other than the simple cylindrical cavity it is possible to simultaneously achieve two important design goals. First, it is possible to enhance the saturated efficiency by profiling the RF field amplitude in the cavity. In general this is achieved by a cavity where the fields increase along the electron beam to the end of the cavity and then drop abruptly. Figure 2.2-4 shows such a cavity shape which was theoretically analyzed<sup>7</sup> and which demonstrated enhanced efficiency in an experimental gyro-monotron.<sup>8</sup>

The second design goal which can be achieved by shaping the cavity is to move the unused eigen modes away from synchronism with the beam mode so that only the desired mode will be excited. As will be shown, this is an important consideration for gyro-monotron design because the cylindrical cavity does not provide sufficient mode separation.

The previously cited Reference 8 discusses mode separation via cavity shaping and provides a theoretical basis for calculating the eigen modes of cavities which have a slowly varying cross section. Also, computer codes exist for numerically simulating the eigen modes in cylindrical cavities with arbitrary shapes.<sup>9</sup>

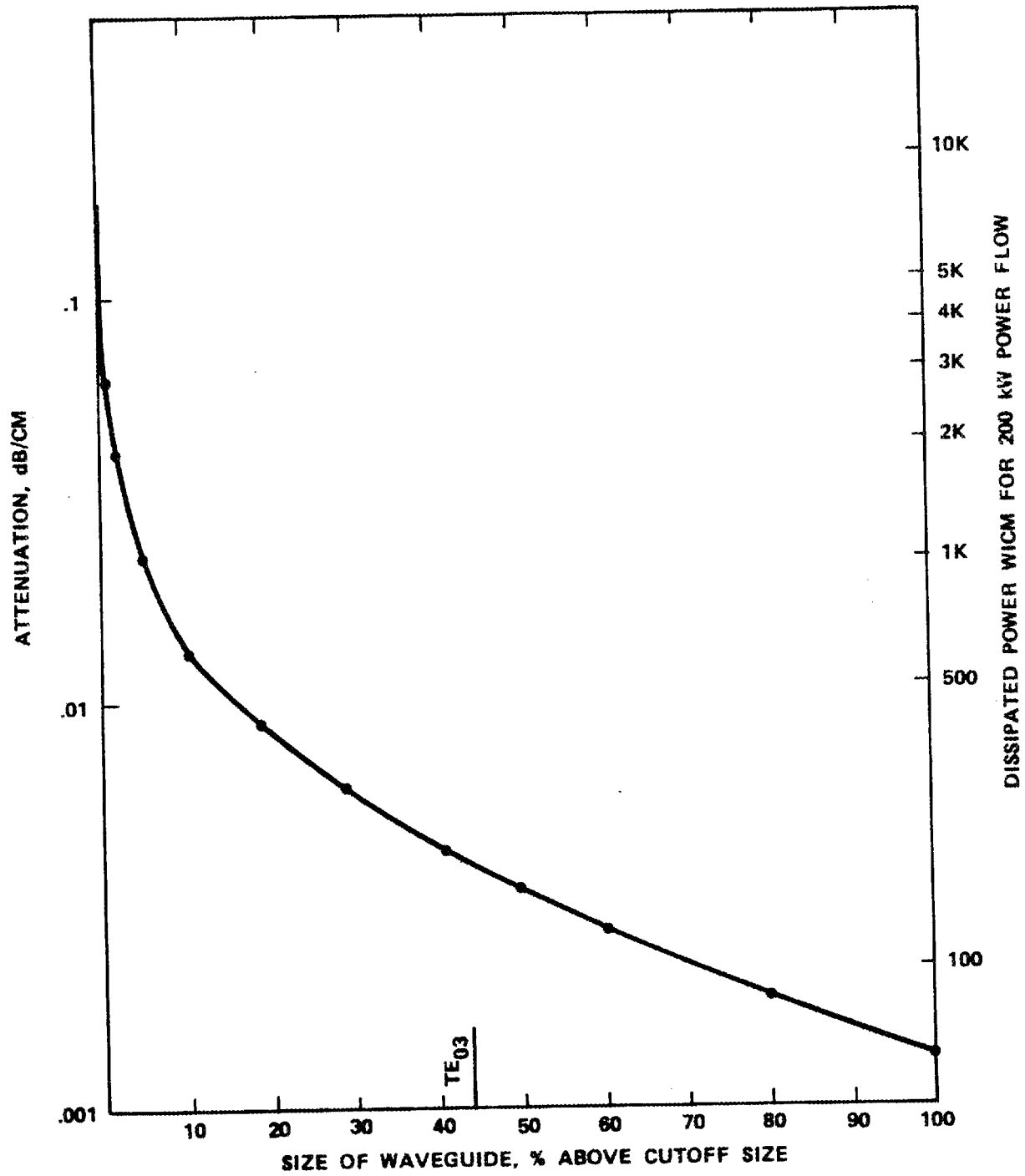


Figure 2.2-3 Attenuation and power loss for  $TE_{02}$  mode as a function of waveguide radius above cut-off.

G5397

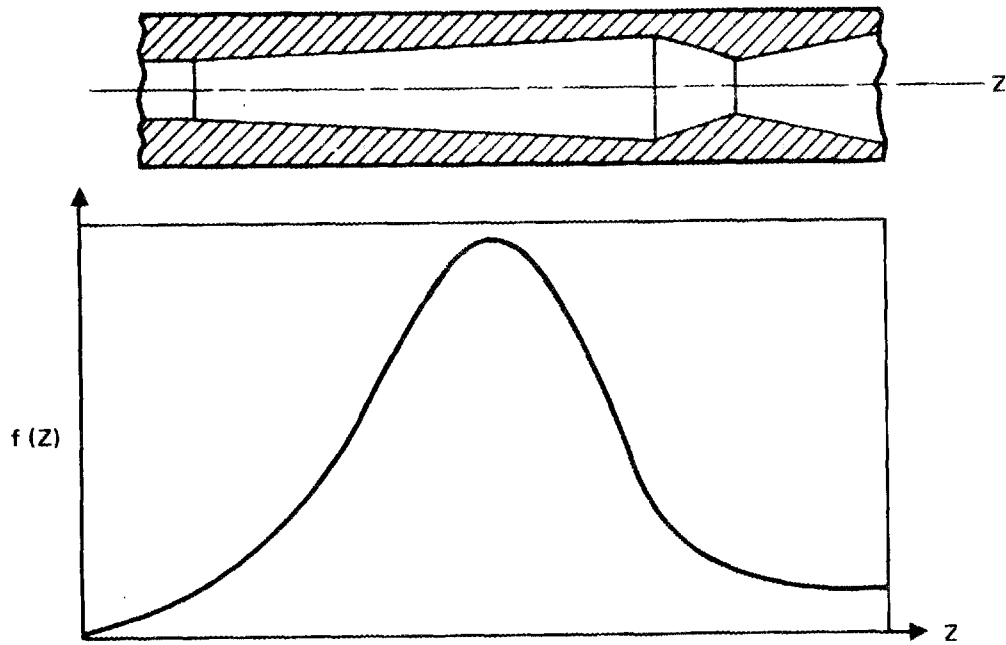


Figure 2.2-4 Shaped gyro-monotron cavity formed by the junction of two conical sections. The function  $f(z)$  gives the  $z$  dependence of the field amplification in the cavity.

As was illustrated in the previous Figure 2.2-2, the dispersion relationship for the beam cyclotron mode is given by

$$\omega_s = k_z v_z + \frac{s\Omega_0}{\gamma_0} \quad (2.2-10)$$

The synchronous case where the beam cyclotron mode passes through the cavity eigen mode is given by

$$k_z v_z + \frac{s\Omega_0}{\gamma_0} = \left[ (ck_z)^2 + (ck_n)^2 \right]^{1/2} = \omega_{nl} \quad (2.2-11)$$

If in addition to this equation we require that

$$\omega_{nl} = \frac{\ell\pi c}{L\beta_z} \quad (2.2-12)$$

we get the condition of tangency between the cyclotron beam mode and the waveguide mode. This condition provides for optimization of the small signal interactions in the cavity, but in general it need not be strictly adhered to if other design requirements so dictate.

It is sometimes desirable, for example, to deviate somewhat from Equation (2.2-12) in order to reduce the possibility of interactions with undesirable modes. Also, large signal analysis usually shows enhanced efficiencies for cavity lengths somewhat longer than the length dictated by Equation (2.2-12). Increasing the cavity radius and magnetic field length, however, has only a small effect on the cavity radius and magnetic field.

In general, Equations (2.2-11) and (2.2-12) provide the starting point for first order design of gyro-monotrons. These equations can be simplified to the following set of design relationships.

$$r_w = \frac{X_n \gamma_z c}{2\pi f}$$

$$\Omega_o = \frac{2\pi f \gamma_o}{\gamma_z^2} \quad (2.2-13)$$

$$L = \frac{c}{2f\beta_z}$$

For a specific example of  $V = 70$  kV,  $\alpha = 1.5$ ,  $s = 0$ ,  $n = 2$ , and  $f = 110$  GHz, Equation (2.2-13) gives the following first order design values respectively.

$$r_w = 3.157 \text{ mm}$$

$$B_o = 41.534 \text{ kG}$$

$$L = 5.177 \text{ mm}$$

We now examine the start oscillation conditions for the gyro-monotron. Chu defines a dimensionless quantity  $F$  to be the rate of the total time average beam energy gain during one transit time ( $\tau = L/v_z$ ) to the total stored field energy,

$$F = \frac{\Delta P_b \tau}{W_f} \quad (2.2-14)$$

and shows that in the small signal approximation for a cylindrical cavity, this quantity can be calculated from the basic parameters of the beam and RF cavity.

The factor  $F$  can then be used to calculate the small signal start-oscillation conditions for the oscillator as follows. The rate at which the beam supplies power to the cavity is given by

$$P_{in} = \Delta P_b = - \frac{FW_f}{\tau}$$

while the rate at which power leaves the cavity is

$$P_{out} = \frac{\omega W_f}{Q} \quad (2.2-15)$$

Defining threshold as the point at which  $P_{in} = P_{out}$  we get

$$- FQ = \omega \tau \quad (2.2-16)$$

By using the beam power  $P_b = N(\gamma_o - 1) m_o c^2 v_z$  and by defining  $P_b^{th}$  as threshold beam power required for oscillations, this can be rewritten as

$$P_b^{th} = \frac{m_o c^2 (\gamma_o - 1) v_z \omega}{(- F/N_T)} \quad (2.2-17)$$

The net result is that for any given set of mode numbers ( $s, n, \ell$ ) and oscillator parameters ( $\bar{\omega}, \Delta, \gamma_o, P_{out}$ ), one can calculate a value of  $P_b^{th}$  for which oscillations will start.

Although the calculation of  $F$  is somewhat cumbersome, our experience seems to indicate that for the important case of maximum saturated

output power, only the  $H_s$  term of  $\alpha_1$  is significant and that the peak of  $-F$  occurs at  $\Delta \simeq \pi$  (for  $s = n = \ell = 1$ ).

Another important feature of Chu's small signal theory is that it provides an estimate for the permissible velocity spread in the beam. Chu shows that for a large range of design conditions the range of  $\Delta$  over which the function  $F$  is negative (i.e., gives up energy to the cavity) is approximately  $2.5 \pi$ . Thus if the axial velocity spread  $\delta\beta_z$  satisfies the relationship

$$\delta\Delta = (\bar{k}_z \delta\beta_z) \bar{r} \ll 2.5 \pi \quad (2.2-18)$$

there will be only a small effect on the efficiency. For the previous 110 GHz design example having a 70 kV beam with  $\alpha = 1.5$ , this turns out to be a relatively lenient criteria.

The basic approach used in the gyro-monotron computer simulation for large signal saturation is similar to that employed in other large signal analysis codes for O-type devices except that the electron motions are fully three dimensional. In the simulation, the trajectories of a set of "test electrons" (up to 1000) are computed as they pass through the dc and RF fields of the device being analyzed. The average energy change of the ensemble is then used to determine the basic efficiency of the energy exchange.

The initial conditions of this ensemble of test electrons are chosen in such a manner that both the spatial and temporal phase distributions of the electrons in the beam are simulated. For example, a full simulation of a gyro-monotron of the type being considered for this program might use 320 electrons distributed in 8 rings with 40 equally spaced electrons around each ring. The rings would then be launched into the gyro-monotron cavity at equally spaced phase intervals over one RF

cycle. Space-charge forces in the electron beam simulation are included in the computer simulation code.

The equations which are integrated to determine the trajectories of the test electrons come from the relativistic force equation

$$\frac{d\vec{U}}{dt} = \frac{e}{m_0} \left( \vec{E} + \vec{U} \times \frac{\vec{B}}{\gamma} \right) \quad (2.2-19)$$

where the relativistic pseudo velocity vector  $\vec{U}$  is defined by

$$\frac{d\vec{X}}{dt} = \frac{\vec{U}}{\gamma}, \quad (2.2-20)$$

$\vec{X}$  is the position vector, and  $\gamma$  is the Lorentz relativistic correction factor given (in terms of U) by

$$\gamma = \sqrt{1 + \frac{U^2}{c^2}}$$

The set of six nonlinear differential equations given in (2.2-19) and (2.2-20) are integrated in a cylindrical coordinate system to give the values of  $(r, \theta, z, \dot{r}, \dot{\theta}, \dot{z})$  as functions of time. The RF fields in the cavity can be calculated either from the analytic eigen modes of the cavity or in the case of a very irregular cavity shape, from a mesh solution technique.

Upon completion of integrating Equations (2.2-19) and (2.2-20) for each test electron as it passes through the RF cavity, the efficiency of energy exchange is given by

$$\eta = \frac{\gamma_0 - \gamma_L}{\gamma_0 - 1} \quad (2.2-21)$$

where  $\gamma_0$  is defined by the initial energy of the electrons,  $m_0 c^2 (\gamma_0 - 1)$ , and  $\gamma_L$  by the average energy of the test electron ensemble after all electrons have passes through the RF cavity at  $z = L$ . This average energy is given by  $m_0 c^2 (\gamma_L - 1)$  where

$$\gamma_L = \frac{1}{N_e} \sum_{i=1}^{N_e} \gamma_i , \quad (2.2-22)$$

$i$  is an electron index, and  $N_e$  is the total number of test electrons.

## REFERENCES FOR SECTION 2.2

1. N. I. Faytsev, T. B. Pankratova, M. I. Peklin and V. A. Flyagin, "Millimeter and Submillimeter Waveband Gyrotrons." Radiotekhnika i Electronica, 1056-1060 (1974).
2. Private conversation with A. Drobot; result based on extensive computer studies at NRL.
3. L. Seftor, A. T. Drogot and K. R. Chu, "An investigation of a magnetron injection gun suitable for use in cyclotron resonance masers." To be published IEEE MTT.
4. K. R. Chu, "Theory of Electron Cyclotron Maser Interactions in a Cavity at Harmonic Frequencies." Naval Research Lab, Washington, D.C., NRL Report No. 3672, April 1978.
5. R. E. Collin, Foundations of Microwave Engineering, McGraw-Hill, N.Y. 1966, p. 327.
6. R. E. Collin, Field Theory of Guided Wave, McGraw-Hill, N.Y. 1960 pp 195-198.
7. S. N. Vlasov, et al., "Open Resonators in the form of waveguides of variable cross section," Radiofizika, Vol 12, pp 1236-1244, 1969.
8. C. V. Kisel, G. S. Korablev, V. G. Navel'yev, M. I. Petelin, and SH. YE. Tsimring, "An Experimental Study of a Gyrotron Operating at the Second Harmonic of the Cyclotron Frequency with Optimized Distribution of the High-Frequency Field" (1973).
9. R. Holsinger, "Poisson Group Programs User's Guide," LBL Internal Report, May 8, 1977.

### 2.3 DESIGN APPROACH

Based on previous experience cited in the literature and our own gyrotron simulations, the design of gyro-monotrons and their associated electron guns at the 200 kW output power level (and 110 GHz) will best be accomplished at beam voltages in the 60 to 80 kV range.

The strongest driving factor to operate at this voltage level is the required beam current and associated cathode loading. A first order design trade-off of the magnetron injection gun shows that at 70 kV with an assumed efficiency of 35%, and  $\alpha = 1.5$ , the cathode loading for a reasonable gun design will be about  $8 \text{ A/cm}^2$ . Any lower beam voltage or higher  $\alpha$  will increase this cathode loading and/or make the gun design more difficult. We have therefore elected to use  $V_0 = 70 \text{ kV}$  and  $\alpha = 1.5$  as electron beam design parameters. These parameters are also consistent with high efficiency for the gyro-monotron.

The electron beam radius in the rf interaction region is determined from a first order rf cavity design. For a cylindrical cavity operating in the  $\text{TE}_{021}$  mode the cavity radius is 3.055 mm and the average beam radius required to optimize the rf interaction with this mode is  $b_0 = 0.26 r_w = 0.80 \text{ mm}$ . The cyclotron radius of the electron motion will be 0.18 mm.

The primary tool for optimization of the design parameters for maximum efficiency is the large-signal Gyro-monotron computer code. This simulation code provides the only practical means for predicting the effects of design changes on the saturated oscillator efficiency and therefore is indispensable both as an initial design tool and as a second iteration refinement tool.

In design optimization, the large-signal analysis code is used to find the optimum set of design parameters which provide the highest efficiency by changing the parameters (within selected constraints) and

observing the results. The primary variables for this optimization are transit phase (magnetic field) and electric field (cavity Q). Thus, for each case of beam voltage and mode geometry, an optimum efficiency can be found as a function of two variables  $A$  and  $E_{\theta 0}$ .

As an example of this procedure we have used the large-signal analysis program to determine the optimum design parameters of a gyro-monotron having a cylindrical cavity geometry. The results are given in Figures 2.3-1 and 2.3-2.

After finding the optimum value of efficiency at  $\bar{E}_{\theta 0} = 0.16$  and  $B/B_0 = 0.967$  ( $B_0$  is the magnetic field value corresponding to  $\Lambda = 0$  for the  $TE_{021}$  mode) the two figures were created by first holding  $B$  constant and varying  $E_0$  and then holding  $E_0$  constant and varying  $B$ . The results indicate a peak efficiency of about 36%.

Note that the  $TE_{021}$  mode is being used rather than the  $TE_{011}$  mode. This has the advantage of delivering a higher peak efficiency (36% instead of 31%) and results in a larger waveguide diameter, reducing heat dissipation. With shaped cavities, efficiencies approaching 40% should be possible using the  $TE_{021}$  mode, assuming stable mode control can be achieved.

The design of an electron gun is dictated by the parameters of the required electron beam and is constrained by factors such as voltage breakdown, maximum cathode loading, and available magnetic field. In a gyrotron gun these parameters include in addition to the geometric and electrical specifications the further restrictions that these parameters be obtained with a specific magnitude of magnetic field and that a given part of the beam's energy be in rotational motion. The design problem is further complicated by the need to minimize the spread in rotational energy.

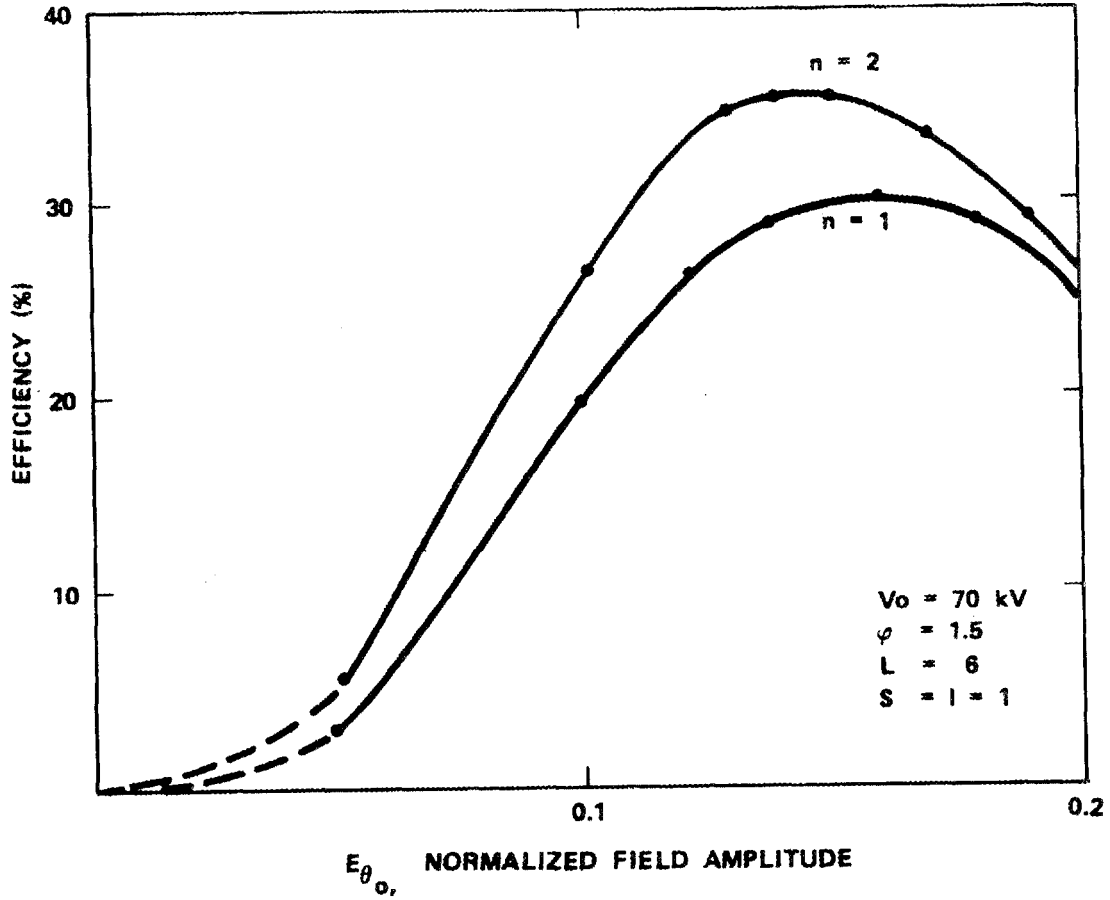


Figure 2.3-1 Efficiency vs cavity field amplitude (cavity Q) for  $B/B_0 = .97$ .

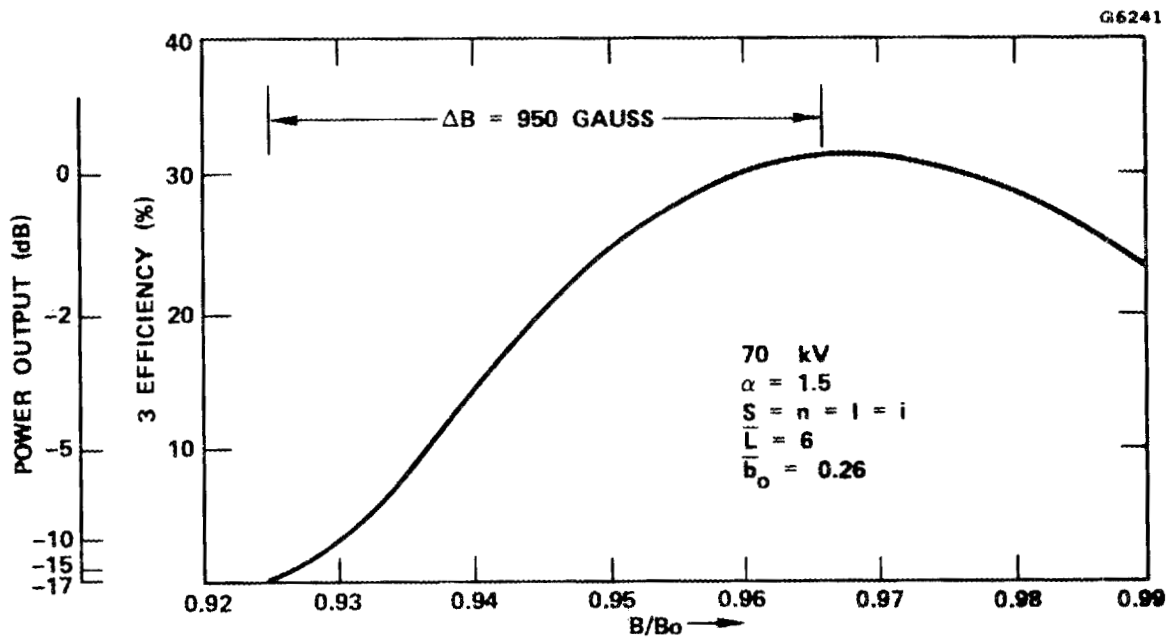


Figure 2.3-2 Efficiency and power output (dB) versus magnetic field for constant  $E_0$ .

In a typical magnetron injection gun, the extraction of the electrons depends on the presence of a magnetic field at the cathode. Unfortunately this magnetic field plays a considerable role in determining the subsequent electron motion and therefore restricts the options available to the designer. Specifically, the energy in rotation in the magnetic field imparted to the electrons in the gun is related to the energy in the magnetic field downstream by the "transverse adiabatic invariant" and by the need to conserve angular momentum.

The gun geometry is determined to a great extent by the available density of emission from the cathode, and this parameter is left to the discretion of the designer. Electron guns are normally operated in the space-charge-limited regime to avoid the need for highly regulated heater supplies and to minimize emission fluctuations associated with local poisoning.

Gyrotron guns are however operated under temperature limited conditions since it has been found by Tsimring et al.<sup>1,2</sup> that the transverse electron energy spread increases rapidly with increasing space charge. This is confirmed by our own computer simulations of magnetron injection guns with and without space charge. The simulations show that when space charge is introduced into a model a debunching of the trajectories in the cathode region takes place and this causes a spread in the trajectories in the nonuniform accelerating region of the gun and results in a transverse energy spread.

Figure 2.3-3 shows a parameterisation of the gun design for a cathode loading of  $6.0 \text{ A/cm}^2$  and a cone angle of  $\delta = 10^\circ$  and an extraction anode clearance factor of 1.25. It can be seen that for  $r_c = 8.8 \times 10^{-3}$  meter that the equivalent gun operates space charge limited and it is therefore necessary to work with a smaller radius cathode. The correct radius cannot be obtained from this analysis, however, an estimate may be made from the published data of Tsimring<sup>2</sup> which shows the variation in perpendicular velocity  $\Delta v_\perp$  as a function of  $(I_o/I_L)$  for a specific gun design.

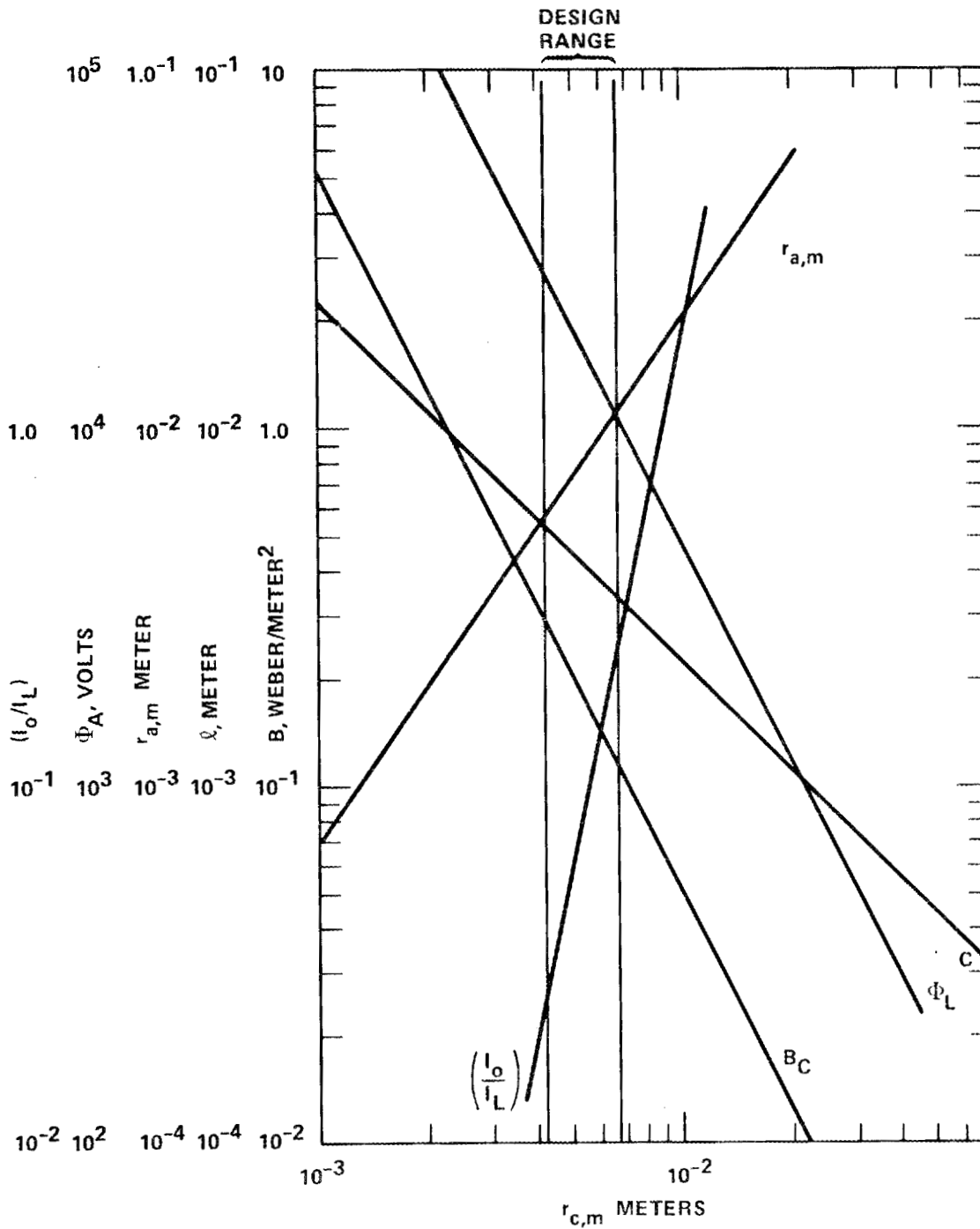


Figure 2.3-3 Design trade-off study of magnetron injection gun.

REFERENCES FOR SECTION 2.3

1. Sh. E. Tsimring, "On the Spread of Velocities in Helical Electron Beams" *Radiofizika*, 15, No. 8, pp. 1247-1259 (1972).
2. E. G. Avdoshin, L. V. Nikolaev, I. N. Platonov and Sh. E. Tsimring, "Experimental Investigation of the Velocity Spread in Helical Electron Beams" *Radiofizika*, 16, No. 4, pp. 605-612 (1973).

### III. PROGRESS

#### 3.1 GENERAL

Effort for this program has been divided into the following tasks:

- RF Circuit
- Electron Gun
- Collector
- Solenoid
- Power Supply
- Beam Analyzer/Tester
- RF Test Equipment

This section describes progress made during the subject period.

#### 3.2 RF CIRCUIT

The RF circuit is a single cavity which will be resonant at 110 GHz for a  $TE_{021}$  mode. The Q of the cavity must be predetermined, since the cavity Q determines the start-oscillation threshold and the saturated output power. Calculation of Q for a right cylindrical cavity is relatively straightforward. However complex cavity shapes require more tedious calculations.

A numerical technique using interactive computer facilities has been developed to rapidly evaluate the efficiency of arbitrarily-shaped cavities. It is known that an optimum choice of longitudinal cavity profile can greatly enhance efficiency through beam pre-bunching in phase space. In examples computed at 30 GHz, use of a 1.2 taper cavity increases mode spacing by 4-7 times (for  $TE_{021}$  and  $TE_{022}$  modes) and can increase the required Q of a cavity by more than a factor of 2. It is

suggested, but not yet demonstrated, that tapering can enhance the efficiency beyond 50%. The effect of the size of input and output beam holes also affects efficiency and Q.

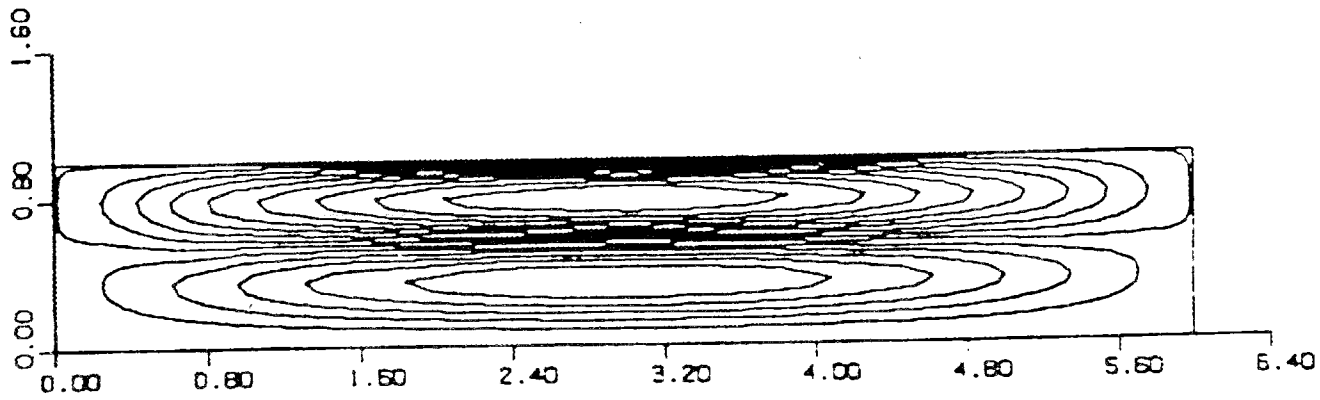
Typical graphical output from the computer program is illustrated in Figure 3.2-1 for a right cylindrical cavity. The contoured lines represent the H fields of a  $TE_{02}$  mode. The E field lines are perpendicular to the plane of the paper, directed into the paper for one peak field and out of the paper for the other peak.

Figure 3.2-1A depicts the desirable  $TE_{021}$  mode, resonant at a frequency of 33.606 GHz, while Figure 3.2-1B shows that the  $TE_{022}$  mode is only 0.282 GHz away. The unloaded Q calculated by the computer program for this cavity is 230.

Figure 3.2-2 illustrates the same modes for a tapered cavity of exactly the same length, only now, the  $TE_{021}$  and  $TE_{022}$  modes are separated by 1.324 GHz. The computed Q for the tapered cavity is 567.

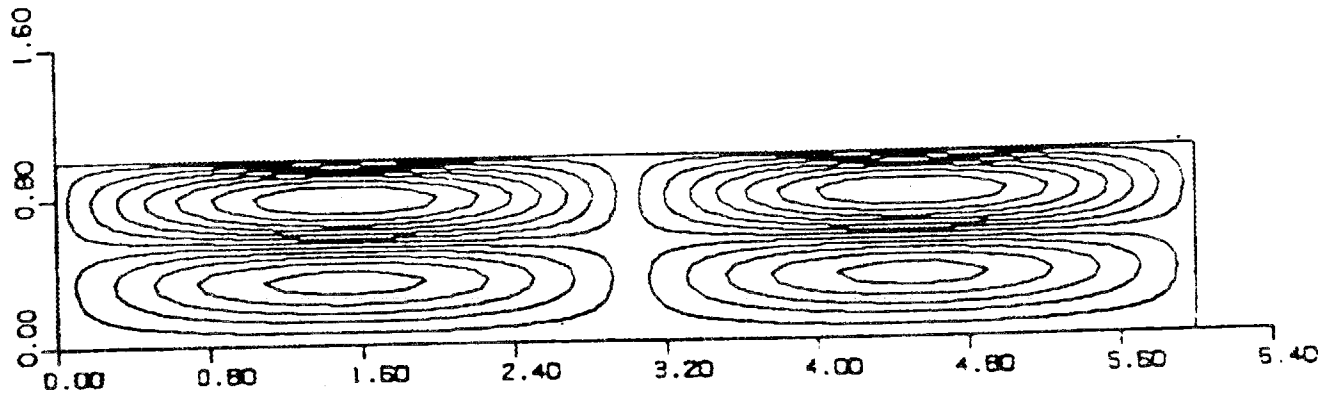
Figures 3.2-1 and 3.2-2 also illustrate that it is theoretically possible to interact with either of the  $TE_{02}$  peak fields. However, the size of the input beam hole, which should be as small as possible to prevent RF from traveling toward the cathode, may preclude the beam reaching the optimum position of the upper peak E fields. The theoretical efficiency which can be attained by interacting with the lower peak in this cavity is 35% and 29% for the upper.

Theoretical in this case implies no variation of spread in  $v_{\perp}$ . However, practical limitations make it impossible to produce a beam without velocity spread. Moreover, a beam made to interact with the more efficient lower mode will have inherently more energy spread because of its higher current density. Alternatively, interacting with the upper



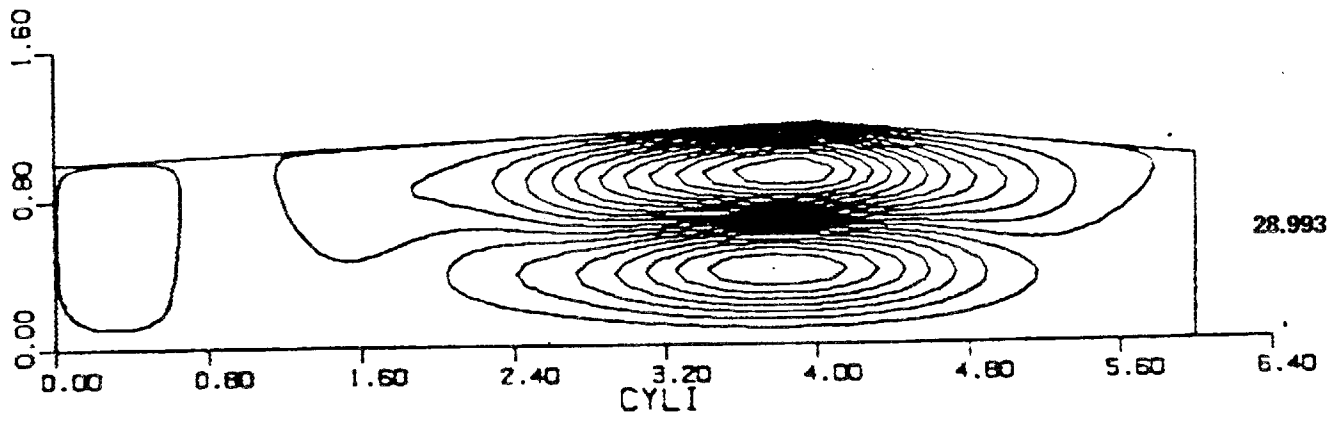
(a)  $TE_{021}$  mode, frequency = 33.606 GHz.

$\Delta f = 0.282$

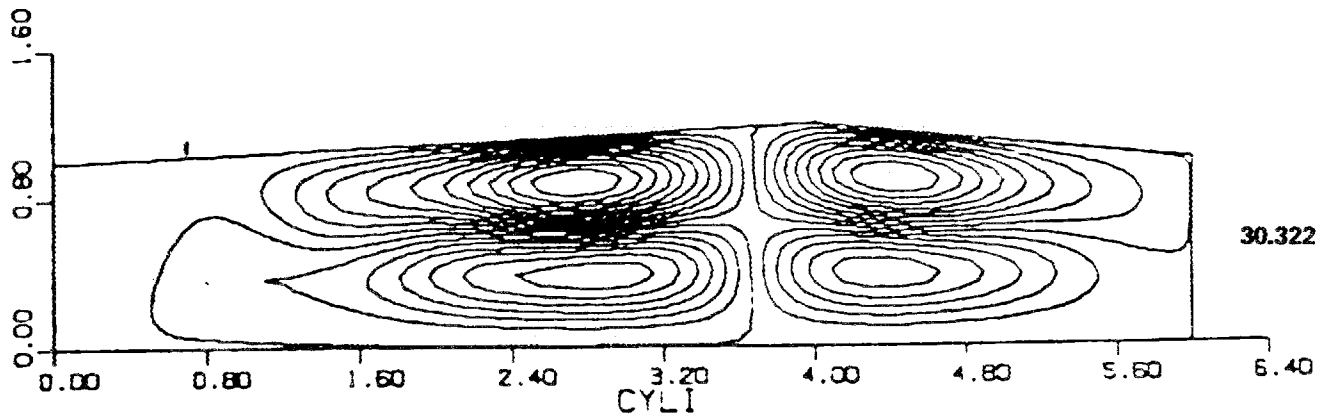


(b)  $TE_{022}$  mode, frequency = 33.888 GHz.

Figure 3.2-1 Field plots for cylindrical cavity showing frequency separation of 0.282 GHz between  $TE_{021}$  and  $TE_{022}$  modes.



(a)  $TE_{021}$  mode, frequency = 28.998 GHz.



(b)  $TE_{022}$  mode, frequency = 30.322 GHz.

$\Delta f = 1.324$

Figure 3.2-2 Field plots of tapered cavity showing frequency separation of 1.324 GHz between  $TE_{021}$  and  $TE_{022}$  modes.

mode will cause the beam to pass close to the cavity walls, in particular to the smaller diameter ends of the cavity which produce an RF short at the resonant frequency. In practice, the cavity need not terminate abruptly; shorter or more gently sloped cavity terminations should be feasible. These configurations are being analyzed.

It is generally recognized that shaping the cavity enhances gyrotron efficiency, as well as providing greater mode separation. Many cavity shapes can be found in the literature, and several have been evaluated with our computer programs. The most promising cavity is shown in Figure 3.2-3. The equipotential lines again show the H fields of the  $TE_{02}$  mode. Figure 3.2-4 shows how beam - RF interaction efficiency grows as the beam passes through this particular cavity. The peak efficiency predicted by the computer program is 34.8%, which is approximately that which could be achieved by a cylindrical cavity. However, the Q, and consequently the mode separation, is significantly higher for the cavity of Figure 3.2-3. Further evaluation of this cavity design will be implemented during the next quarter, including cold testing.

A study was made to determine reliable and accurate methods for making cavity Q measurements, which would serve as a check of the computer program. The methods chosen were transmission method and phase and amplitude input impedance measurements using the polar plot network analyzer.

Methods using complex eigenvalue differential equations were investigated along with analytical methods and the Cavity computer program. From these studies and cold-test experiments, considerable knowledge of cavity design will be available.

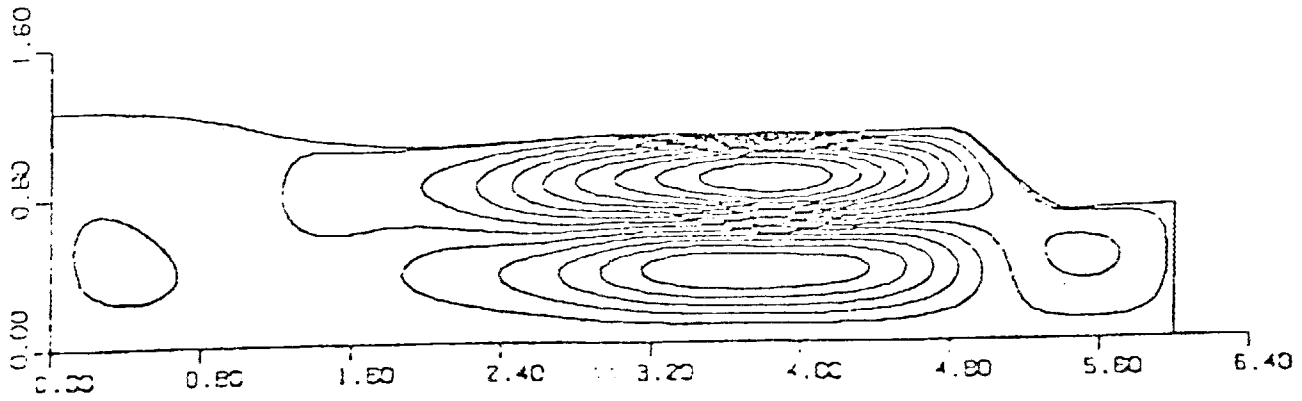


Figure 3.2-3 Shaped cavity design for TE<sub>02</sub> mode.



A set of cavities were drawn up with various shapes and hole sizes and sent out for machining. Some preliminary testing was done to check equipment.

Velocity spread in the cavity is generally recognized as the most important factor in failing to attain the ideal efficiency predicted by most computer programs. Consequently, a large signal computer analysis has been undertaken to determine the effects of non-uniform transverse velocity on the specific design of the 110 GHz gyrotron.

Preliminary results of the large signal analysis on gyrotron efficiency indicate that for a spread of 10% in  $v_{\perp}$ , efficiency will be degraded 20%. That is, the predicted ideal efficiency of 35%, will be reduced to 28%. It is therefore imperative that velocity spread be minimized to as low a level as possible in the final design.

The physical relationship between the RF cavity and the electron beam, positioned at the lower peak of the  $TE_{02}$  mode, is shown in Figure 3.2-5.

### 3.3 ELECTRON GUN

The basic gun configuration used in gyrotrons is the Magnetron Injection Gun (MIG), operating in the temperature-limited region.<sup>1</sup> The object of the design effort is to produce a hollow beam spiralling on guiding centers which correspond in radius to one of the peak E fields in the cavity. The rotational energy in the beam must produce the "design value" of  $v_{\perp}$ , with a minimum variation (spread) in velocity. The spread in  $v_{\perp}$  can be produced, among other reasons, by operating the cathode too close to the space charge-limited region.

The design of the electron gun can be approximated by assuming the cathode and anode form concentric cylinders.<sup>2</sup> Utilizing the appropriate

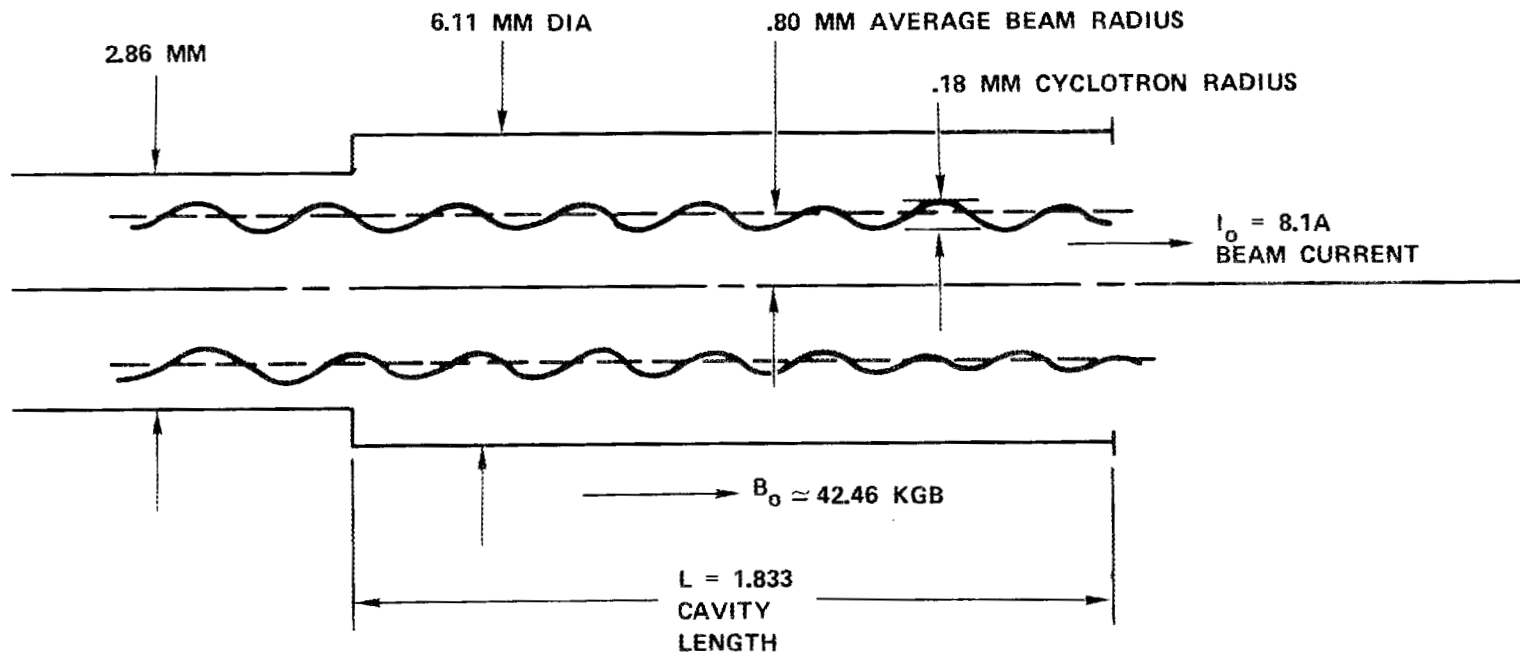


Figure 3.2-5 Scale drawing of beam-cavity geometry for a first order design using a cylindrical cavity.

design values for the lower cavity position (Figure 3.2-5), a computer program was formulated which permits a rapid parametric analysis of various gun configurations. For given final beam parameters, the program provides characteristics of the gun, such as the width of the cathode strip, anode voltage and magnetic field at the cathode. In addition the program calculates the ratio of temperature - limited beam current to space charge-limited current ( $I_o/I_L$ ), which represents how close the cathode is to space charge limited operation.

In Section 2.3 of this report, a graphic representation of the output of the computer program is shown (Figure 2.3-3), wherein, the ratio of anode radius to cathode radius is fixed ( $r_a/r_c = 1.7$ ), and the cathode angle and current density are fixed at  $10^\circ$  and  $6 \text{ A/cm}^2$ , respectively. It can be seen from Figure 2.3-3 that the most variable parameter of magnetron gun design is the ratio  $I_o/I_L$ , whereas cathode magnetic field and anode voltage are not crucial, first-order, tradeoff parameters.

The historical importance of  $I_o/I_L$  has prompted a more detailed analysis, in which the cathode angle and current density are not fixed. The results of this analysis are shown in Figure 3.3-1 for a beam interacting with the lower peak  $\bar{E}$  field in the cavity.

In order to maintain a low ratio of  $I_o/I_L$ ,  $<10\%$ , either the cathode angle should be greater than  $10^\circ$ , or the current density should be increased to excessive values. But, at high values of cathode angle, voltage breakdown or anode interception can occur, and this is shown as the dashed lines of Figure 3.3-1. In fact, at higher cathode angles, the validity of using concentric cylinder theory is questionable. At low cathode angles, around  $5^\circ$ , the cathode can only be operated space charge-limited.

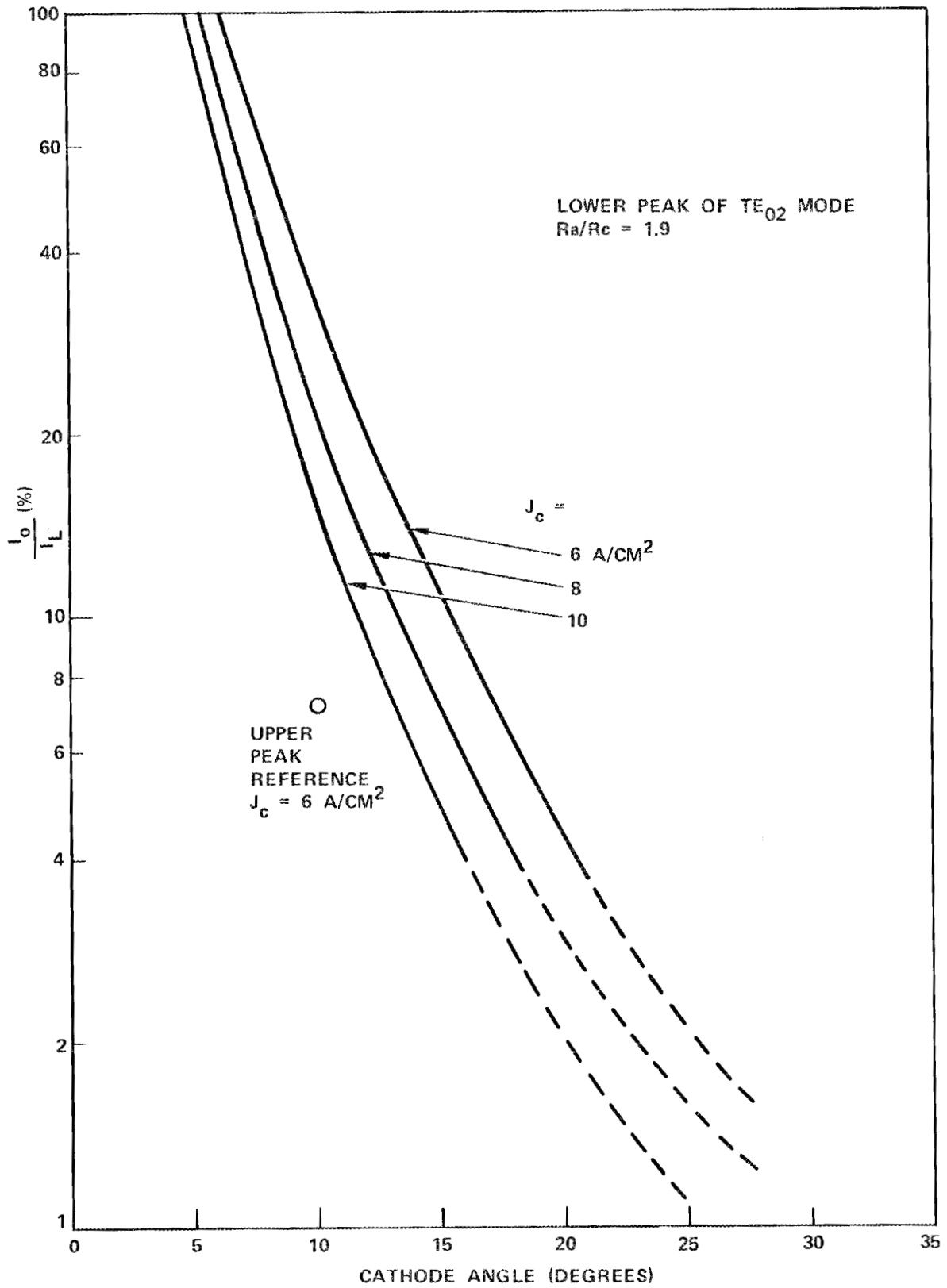


Figure 3.3-1 Emission ratio vs cathode angle.

In contrast, for interaction with the upper peak of the  $TE_{02}$  mode, a reasonable gun can be constructed with a  $10^\circ$  cathode angle and  $6 \text{ A/cm}^2$  current density, while operating at only 7.2% of the space charge - limited current. The disadvantage of interacting with the upper peak field however is lower efficiency. This gun design for the upper field is being explored only as an alternative.

It should be noted, that the effect of other values of  $r_a/r_c$  is to produce only a slight displacement of the curves, to the left for higher values of  $r_a/r_c$ .

The values used in plotting Figure 3.3-1 are those for the smallest possible cathode radius, which just allows the first electron cyclotron orbit to clear the cathode. This value of  $r_c$  produces the lowest ratio of  $I_o/I_L$ . A potential problem associated with the smallest value of  $r_c$  is that the width of the cathode is typically 10-30% larger than  $r_c$ . (See Figure 2.3-3 for small  $r_c$ .) This presents a problem in that electrons leaving from widely spaced positions along the cathode could not reasonably be expected to have the same transverse velocity in the cavity. Successfully constructed gyrotrons have typically had the cathode width,  $\ell$ , equal to  $1/2$  or less of  $r_c$ .

A reasonable tradeoff can be achieved by compromising  $r_c$ ,  $J_c$ , and cathode angle. Figure 3.3-2 illustrates a typical output from one case of the previously described parametric analysis. The current density,  $J_c$ , in this case is  $8 \text{ A/cm}^2$ , a high value not usually employed in microwave tubes. However, at Hughes, M type cathodes, operating in the temperature-limited region, have exceeded 1000 hours of life. Therefore,  $8 \text{ A/cm}^2$  represents a reasonable tradeoff value which results in low  $I_o/I_L$  and relatively long life.

ORNL 110 GHZ GYROTRON

BEAM VOLTAGE = 70000. VOLTS  
 BEAM CURRENT = 8.100 AMPS  
 CATHODE CURRENT DENSITY = 8.00 AMPS/CM2  
 MAGNETIC FIELD = 42460. GAUSS

UPERP/UZ = 1.500  
 CAVITY WALL RADIUS = 0.30560 CM  
 BEAM CAVITY POSITION = LOWER

RA/RC = 1.900  
 GUIDING CENTER = 0.0802 CM

CATHODE ANGLE = 13.25 DEGREES  
 CYCLOTRON RADIUS = 0.0181 CM

CATHODE RADIUS	CATHODE LENGTH	CATHODE MAG FIELD	ANODE VOLTS	ANODE RADIUS	EMISSION FACTOR	VOLTAGE GRADIENT
0.3825	0.4213	1771.7622	17862.6133	0.7267	0.0993	50.1828
0.4207	0.3831	1464.6165	14766.0156	0.7992	0.1599	37.7166
0.4589	0.3512	1230.9299	12410.0117	0.8718	0.2469	29.0600
0.4970	0.3242	1049.0161	10576.0039	0.9444	0.3683	22.8623
0.5352	0.3011	904.6387	9120.4141	1.0170	0.5333	18.3088
0.5734	0.2810	788.1396	7945.8984	1.0895	0.7527	14.8885
0.6116	0.2635	692.7764	6984.4453	1.1621	1.0391	12.2697

Figure 3.3-2 Sample computer print-out from parametric study.

A magnetron injection gun was designed using the parameters of Figure 3.3-2. A magnetic field, producing approximately 1300 gauss in the cathode region and 42,460 gauss in the cavity, was designed using computer-aided techniques. The criteria for designing the magnetic field for this gun were to provide a linear field over the cathode, produce a slow field increase in the beam acceleration region, have less than 0.1% variation in the cavity region, and finally, to provide the required field using realistic current density in the field-producing coils. The effect of these design criteria was that the required spacing between cathode and cavity must be approximately 23 cm.

The gun design was evaluated using a relativistic beam trajectory computer program. The results of the initial design effort are reproduced in Figure 3.3-3. The calculated transverse velocity ( $v_{\perp}$ ) spread was 25%.

The variation in  $v_{\perp}$  was large enough that some electrons emitted from the front (nose) of the cathode had all of their forward longitudinal energy converted to transverse energy, which resulted in those electrons being reflected back toward the cathode.

The apparent reason for this large velocity spread is due to the long cathode width compared to its radius ( $l/r_c \approx 0.8$ ). Electrons near the nose of the cathode are accelerated much more rapidly than those toward the rear. Recognition of this fact led to a modification of the cathode region which provides considerable reduction in  $v_{\perp}$  spread. The modified design is shown in Figure 3.3-4. The shaped center electrode produces lower acceleration for those electrons closer to the nose and higher acceleration for those electrons toward the rear. The computed  $v_{\perp}$  spread in the cavity region is 8%. While the gun design is by no means finalized, this value of  $v_{\perp}$  spread is believed to be adequate, since a 10% spread will still yield efficiency of 28%.

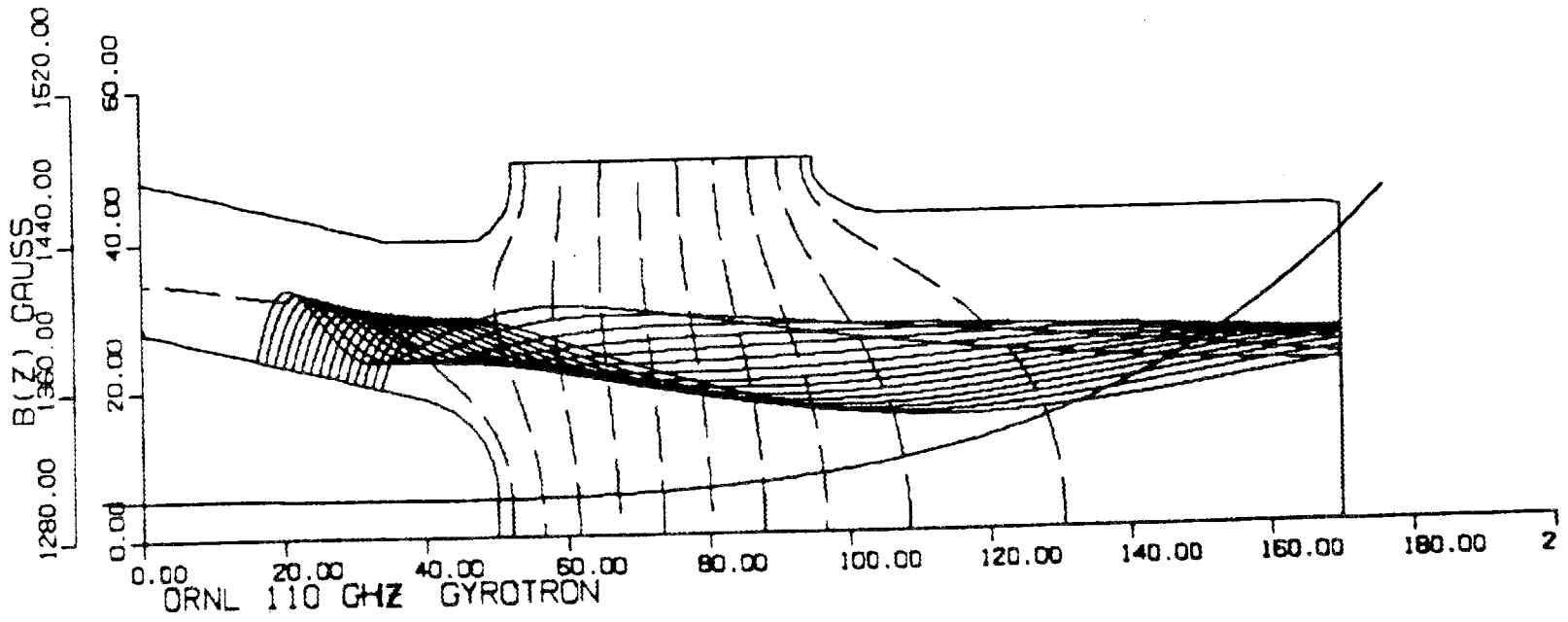


Figure 3.3-3 Conventional magnetron injection gun (A thru F).

Figure 3.3-3A Gun section.

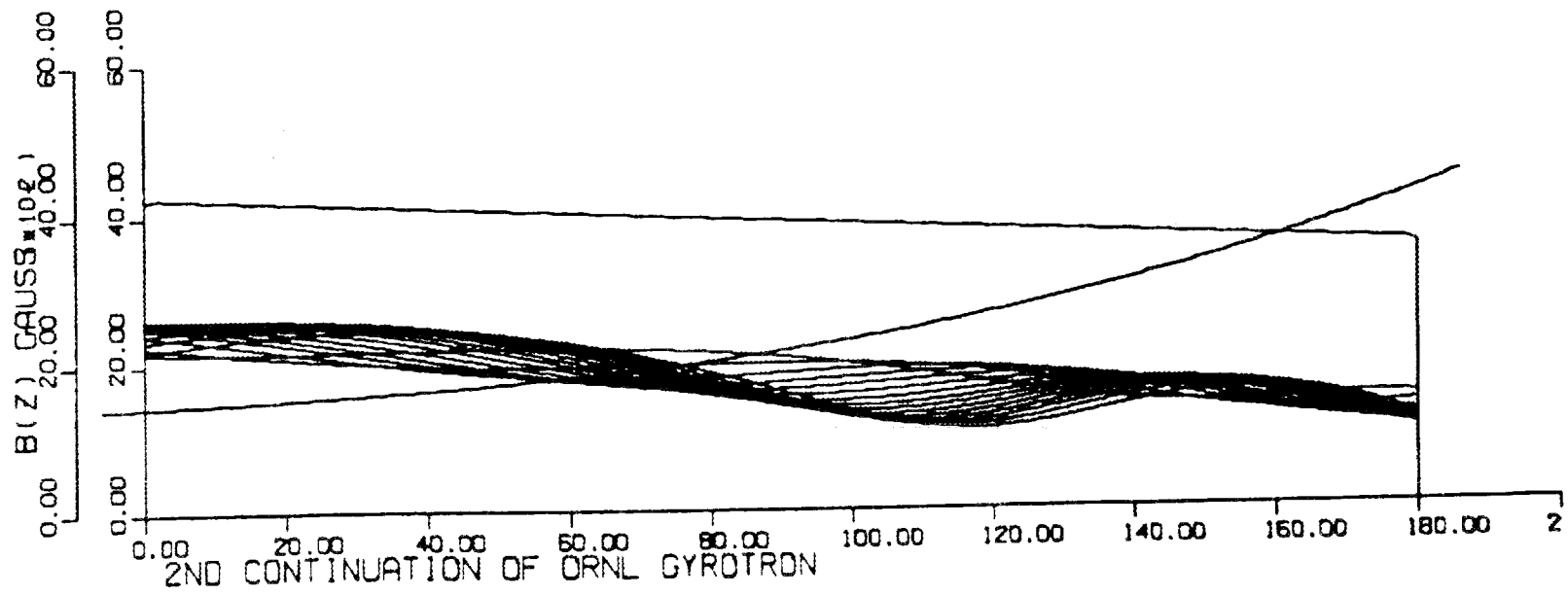


Figure 3.3-3B

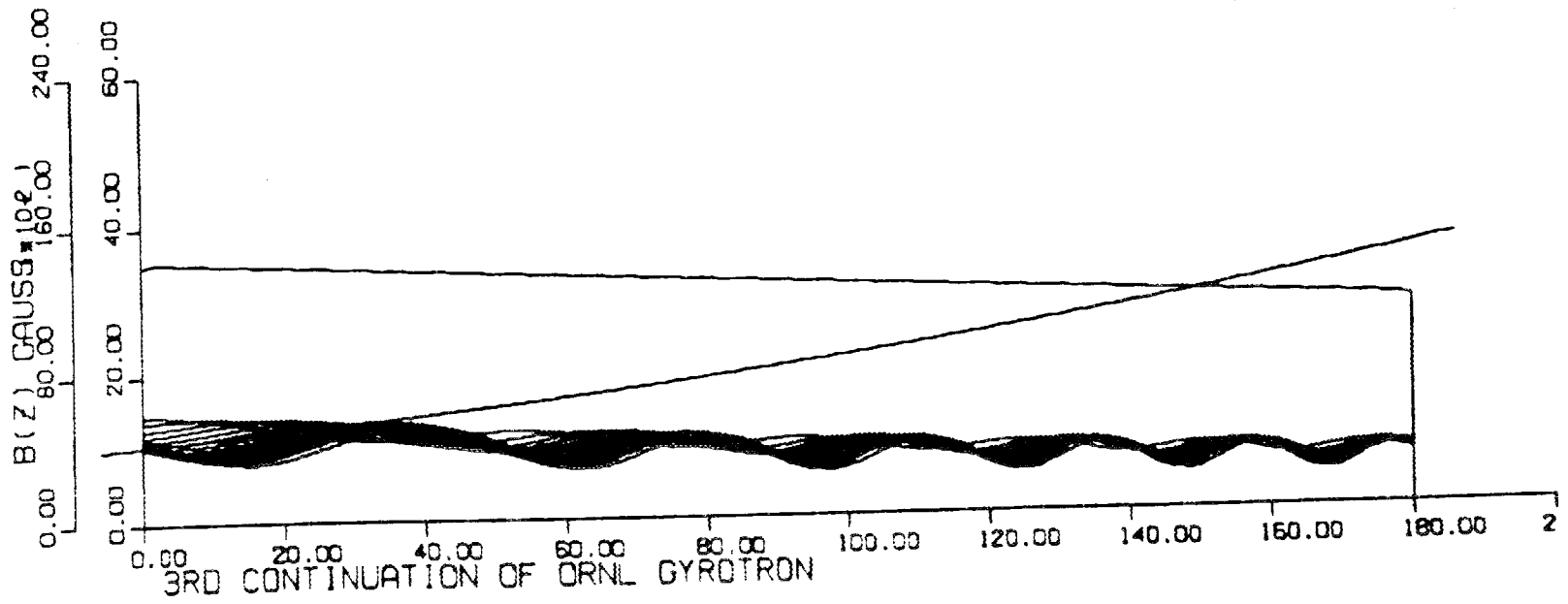


Figure 3.3-3C

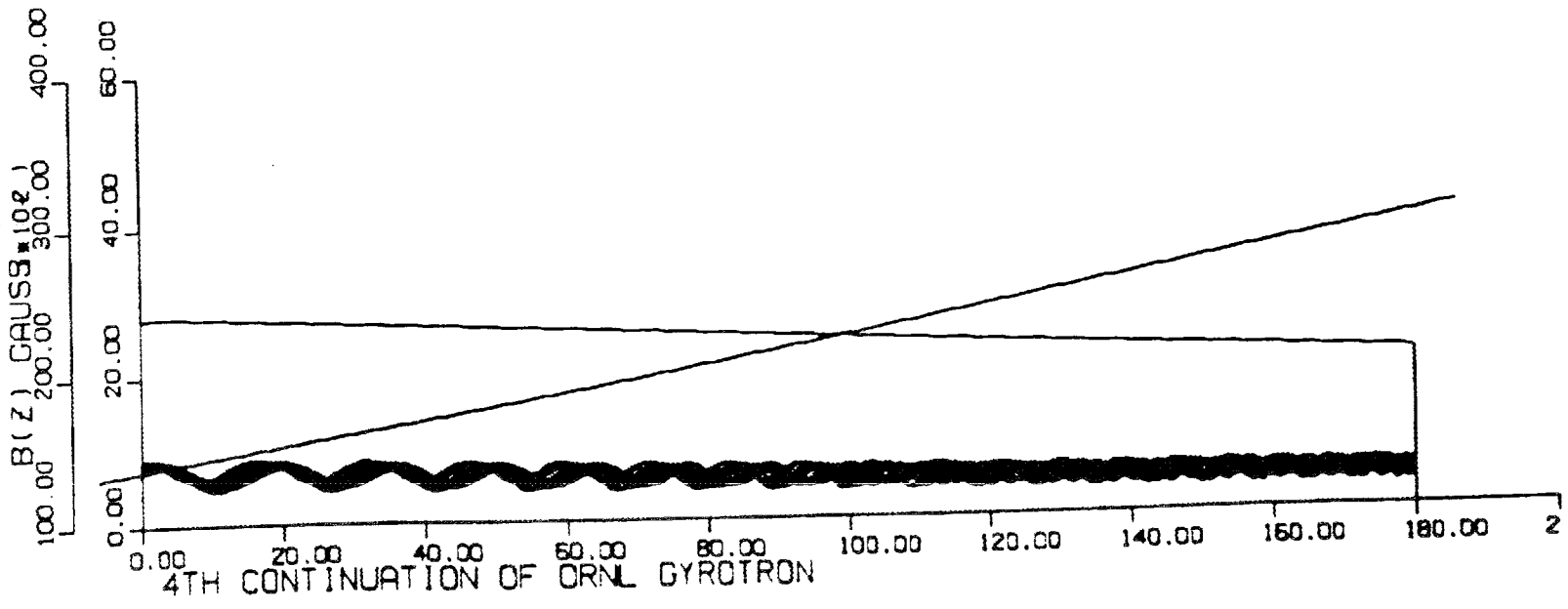


Figure 3.3-3D

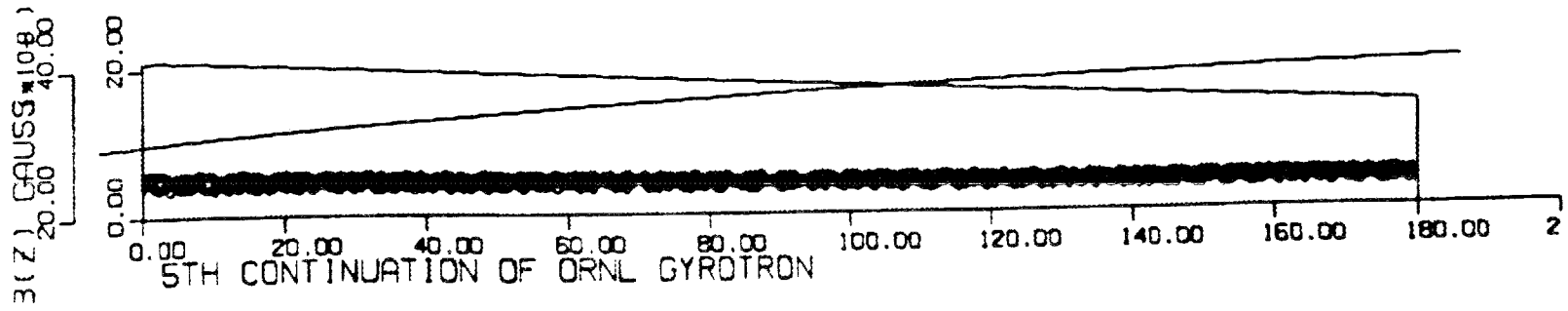


Figure 3.3-3E

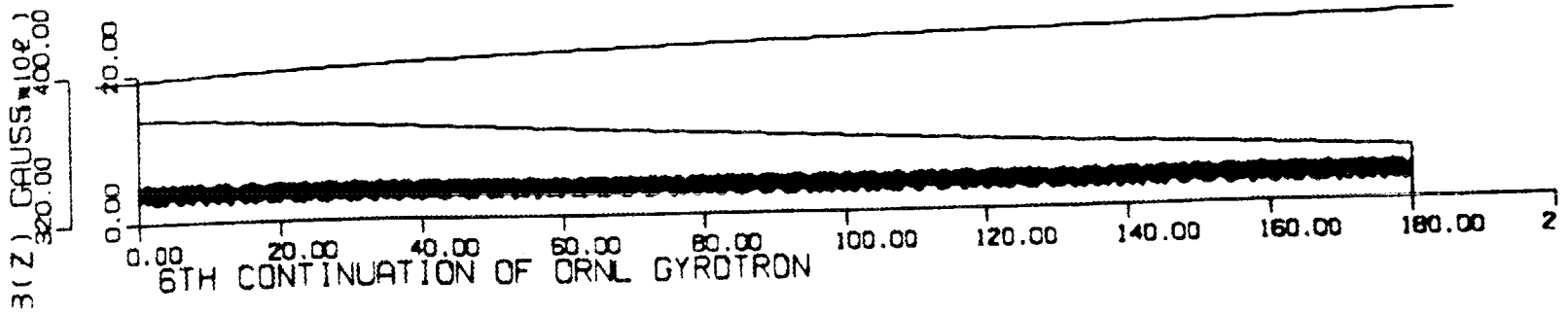


Figure 3.3-3F

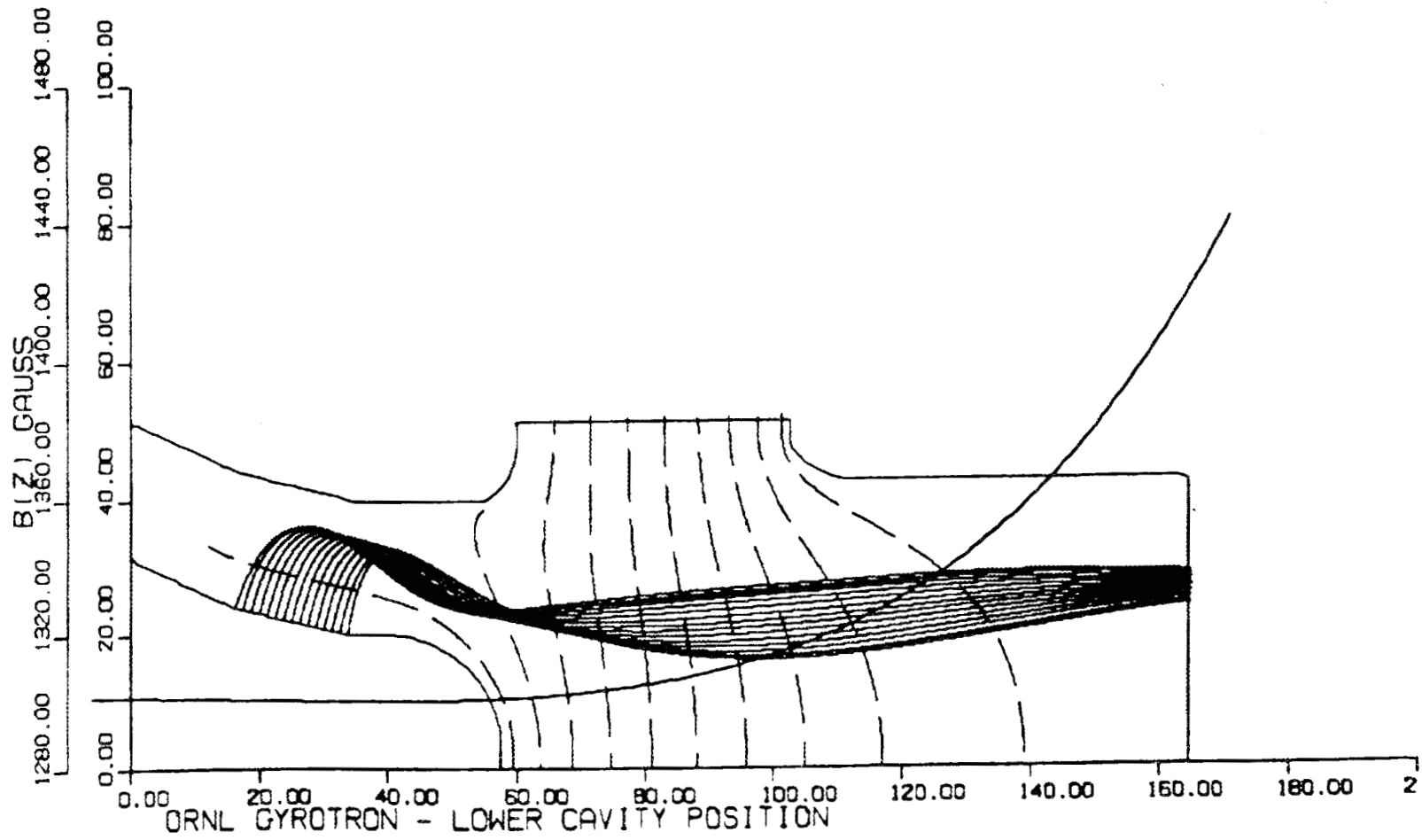


Figure 3.3-4 Modified magnetron injection gun (A thru G).  
Figure 3.3-4A Gun section.

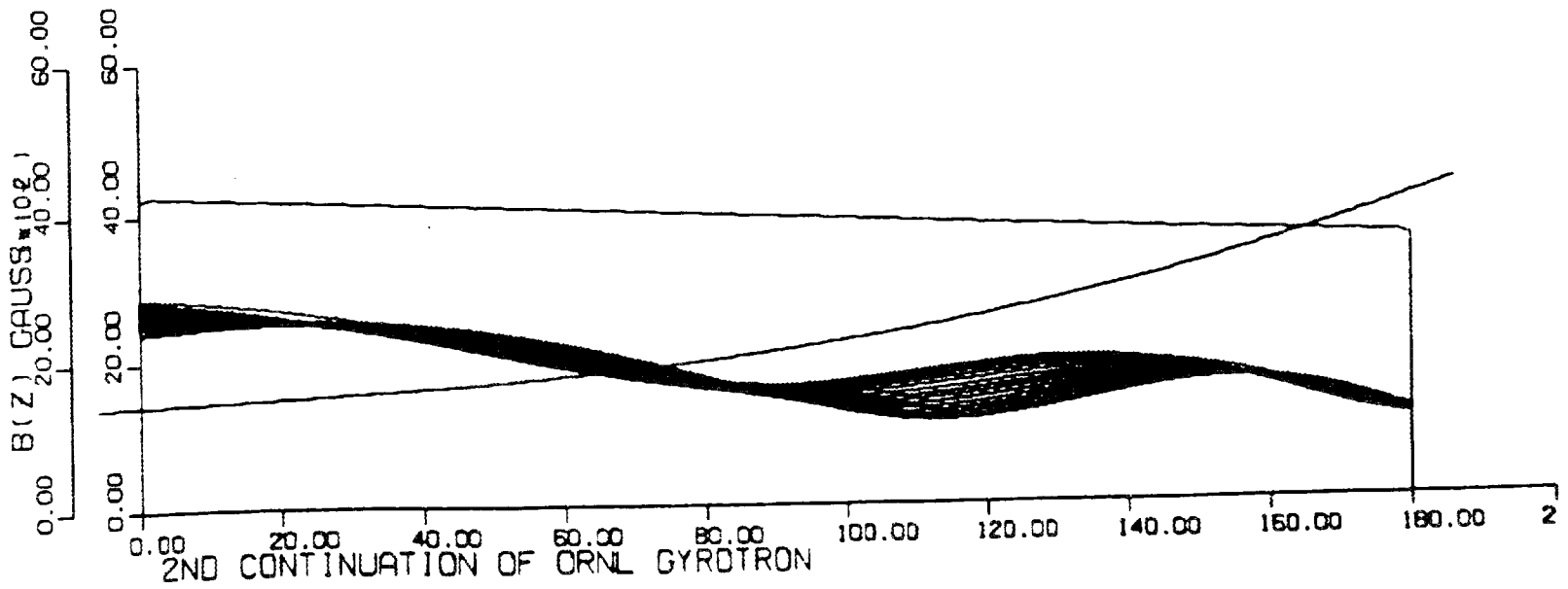


Figure 3.3-4B

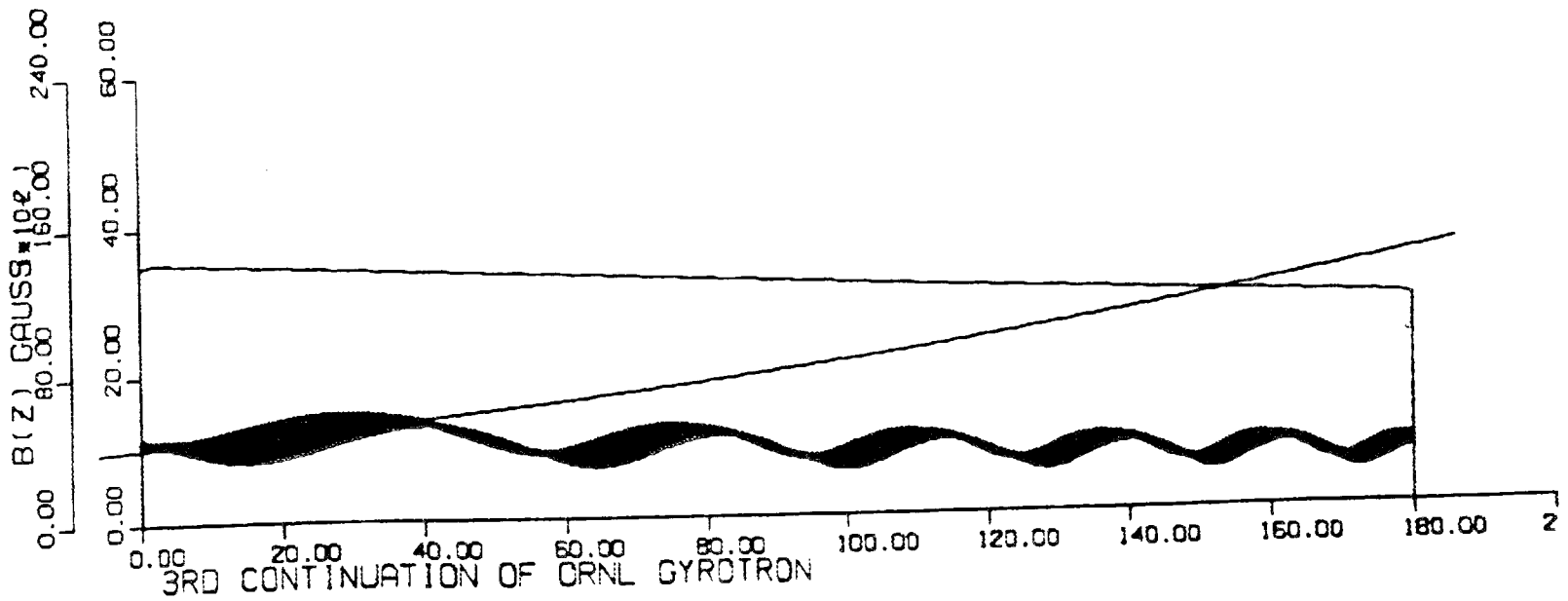


Figure 3.3-4C

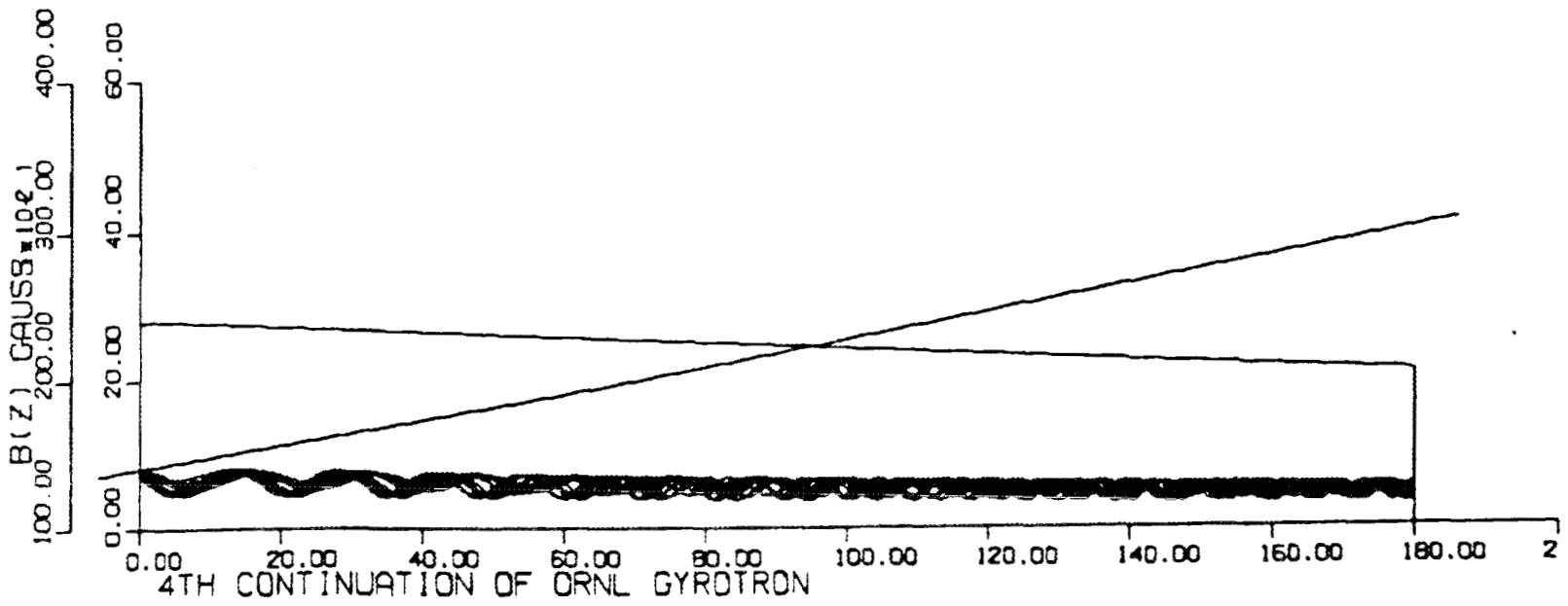


Figure 3.3-4D

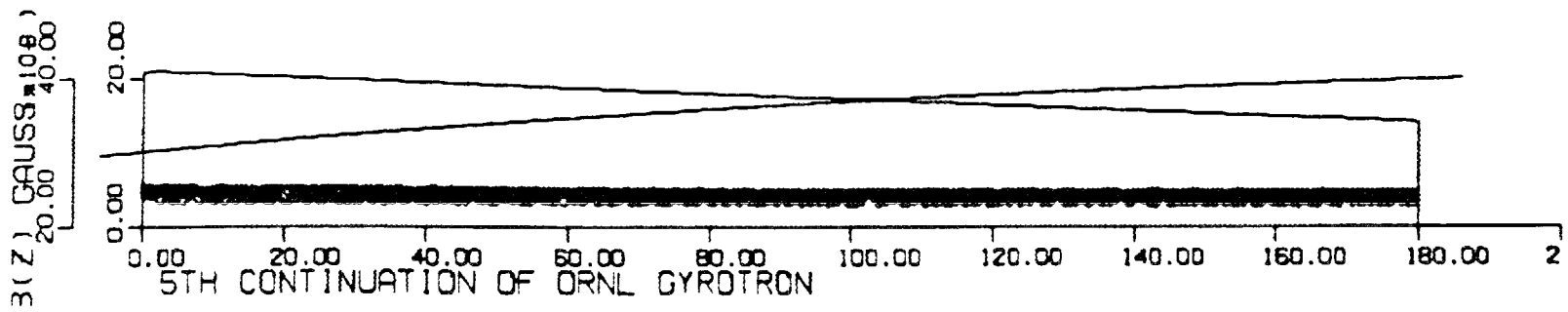


Figure 3.3-4E

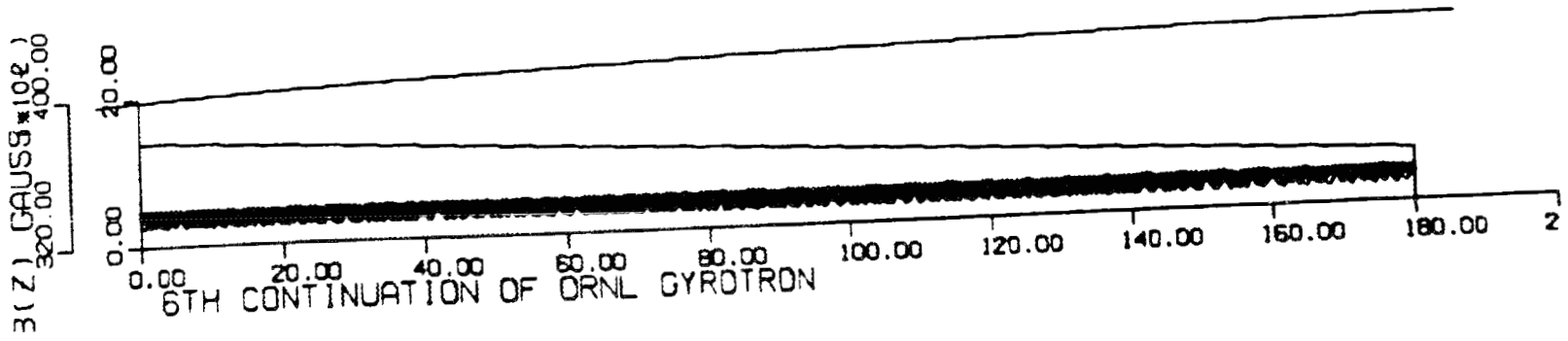


Figure 3.3-4F

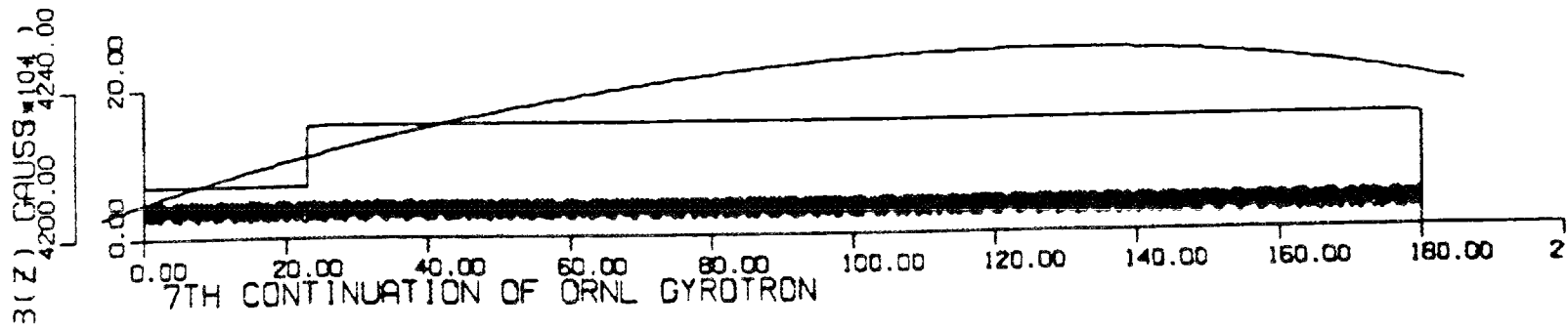


Figure 3.3-4G Cavity region.

### 3.4 COLLECTOR

Two approaches for collecting the beam are being evaluated: the classical, axisymmetric collector and a collector which uses spherical mirrors to separate beam from RF power. In the first design configuration, illustrated in Figure 3.4-1, RF exits through the extreme end of the collector and the beam is collected on the cylindrical walls. The collector essentially begins immediately after the RF cavity. The circular waveguide walls will be smoothly tapered to a sufficiently wide diameter at which the beam may safely be collected. The waveguide walls will then taper down to the size of the RF window. The area over which the beam is collected is dependent upon adequate cooling of the copper walls. The spent beam must be made to diverge magnetically and spread over a conveniently large surface area. This collector design is the most expedient means to obtain the first tube.

Tapering of the collector walls to a larger radius can cause the propagating RF to transfer its power to higher order modes. A method designed to minimize RF moding problems using spherical mirrors has been proposed by R. Dandl<sup>3,4</sup> of Oak Ridge which involves the use of two antennas facing each other as shown conceptually in Figure 3.4-2. In this scheme the electrons are brought out radially between their antennae. This scheme requires a strongly varying magnetic field along which the electrons maintain their cyclotron orbits. The use of a ceramic insulator between the collector and the tube body allows the collector to be depressed with respect to the tube body. This has two advantages, the beam collected is not only at lower energy but also a weaker cusp magnetic field is required to spread out the beam. Further, if for example the cathode voltage was -35 kV with respect to ground, and the tube anode and body was +35 kV with respect to ground, the collector and output window would be at ground potential. The collector would be depressed by 35 kV with respect to the tube body. Opening up the diameter at which the electrons

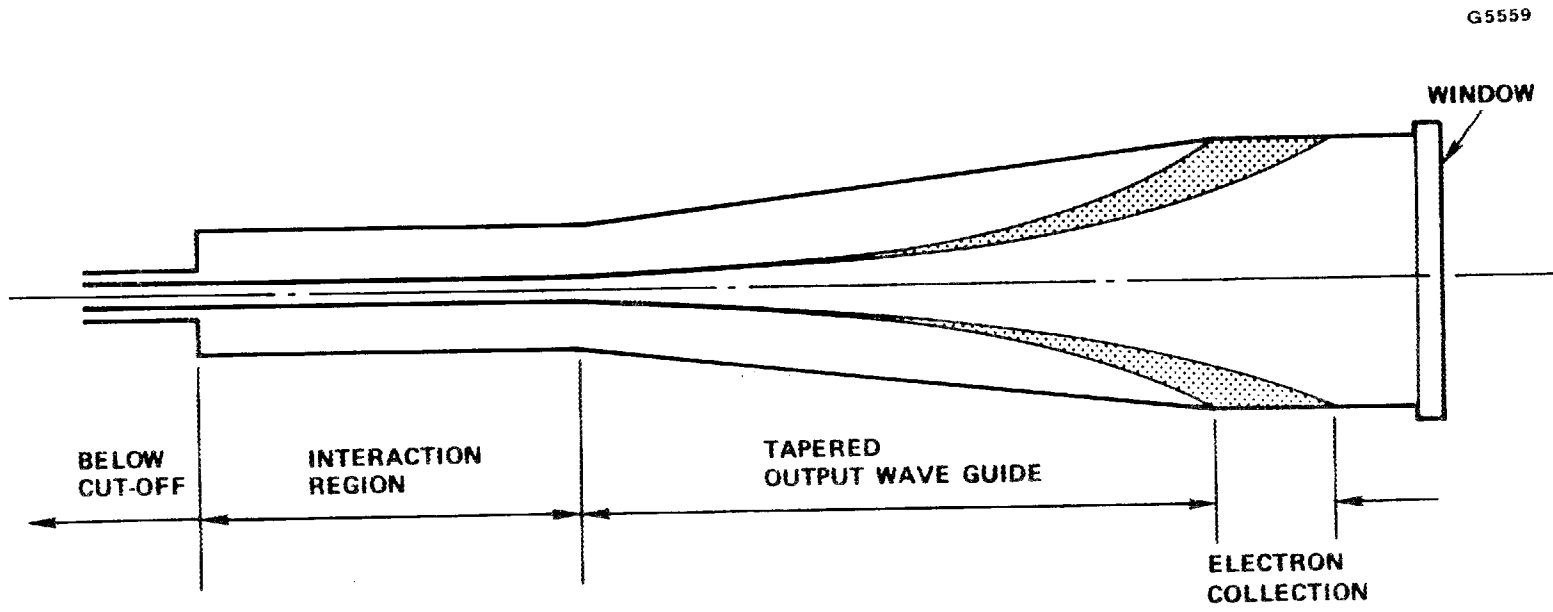


Figure 3.4-1 Schematic of waveguide and electron collector.

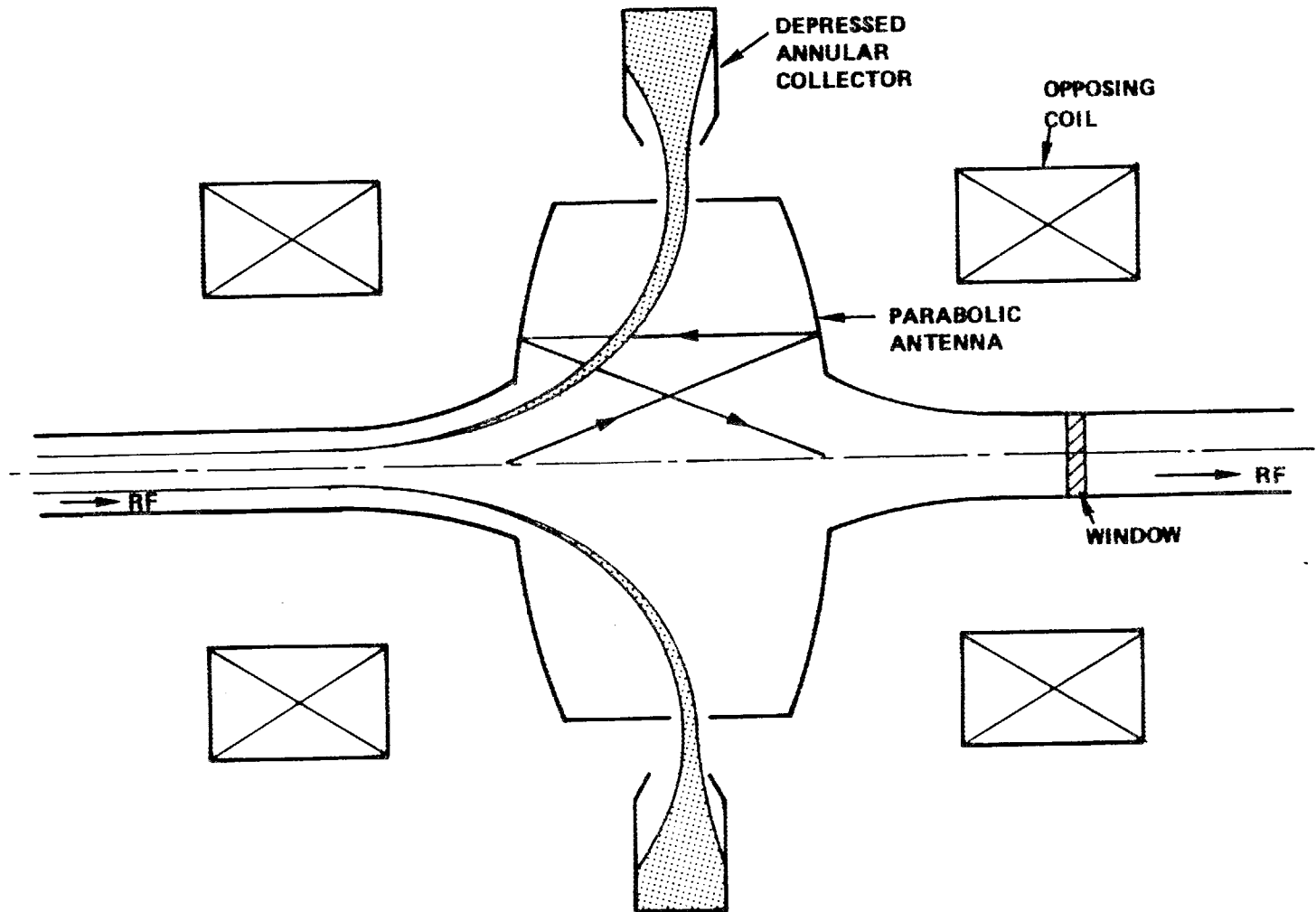


Figure 3.4-2 Electron extraction between facing parabolic antenna proposed by R. Randl of Oak Ridge.

are collected easily allows the attainment of the required area, for easy heat dissipation by liquid-cooled fins.

A disadvantage of this latter scheme is that, at 110 GHz, the tolerance on the mirror surface creates a critical design and manufacturing problem, especially when one considers thermal expansion due to high RF and beam power in the collector region. This collector concept will require careful evaluation before being implemented.

The major issue to be addressed in collector design is power dissipation. Techniques are readily available for dissipating power densities of  $1 \text{ kW/cm}^2$ . In order to evaluate the power density within the axisymmetric collector which will be designed for this gyrotron, the gun design should be finalized. The beam characteristics in the cavity, including anticipated velocity spread, are then analyzed with the large signal computer program to determine remaining energy in the beam. The exiting beam characteristics from the large signal program are then used as input to the beam trajectory program so that power density in the collector region can be evaluated.

It is anticipated that several iterations of collector magnetic field may be required before the power density can be optimized. A pole piece may be required to assist the dispersion of the beam. Once the collector radius is known, the collector will be redesigned as an RF circular waveguide using established techniques.<sup>5</sup>

### 3.5 SOLENOID

The peak magnetic field required in the cavity region is 42,460 gauss. It is anticipated that this field will be obtained with a superconducting magnet. The design established thus far for use in the gun-cavity trajectory plots employs five coils wound on a 5 cm mandrel.

The coil current density is less than  $30,000 \text{ A/cm}^2$ , which represents an upper limit for practical superconducting coils. The field in the cavity varies less than 0.1%.

Over the cathode, a field of 1300 gauss is used in the present gun design. This field is constant to within 1%. No pole-piece is required in the gun region.

The spacing of the coils is such as to provide a slow rising field in the gun region as well as to maintain reasonable coil current densities.

The remaining part of the solenoid design concerns the collector region and an optimum decay of the magnetic field. Once the gun design is finalized, trajectory computations within the collector will be undertaken in order to evaluate the superimposed magnetic field. This evaluation will include the use of collector pole pieces and/or auxiliary, non-superconducting bucking coils.

### 3.6 POWER SUPPLY

A dedicated power supply is necessary for operation of the gyrotron. Salient features of this power supply are given in Table 3-1. A complete specification has been written and sent to ORNL for approval, before proceeding to solicit bids. The estimated delivery date is 12 months ARO. Until the power supply is delivered, testing will be done with 10  $\mu\text{s}$  pulses and at low duty.

TABLE 3-1

Cathode voltage	-100 kV max
Cathode current	10 A max
Control anode voltage	35 kV max
Control anode current	0.2 A
Control anode modes	20-50 $\mu$ s pulse 10 ms-10 sec pulse CW
Body/cavity voltage	Ground
Body/cavity current	2 A max
Collector voltage	-50 kV to ground
Collector current	10 A max
Heater voltage	15 V AC max
Heater current	15 A max
Primary voltage	4160 V 3 phase

Capable of being operated from a remote control panel.

### 3.7 BEAM ANALYZER/TESTER

Knowledge of the actual beam geometry is important to prevent circuit overheating due to beam interception and to evaluate gun circuit and collector performance, as well as construction techniques. Determination of the electron velocity spread in the beam is necessary to optimize the gyrotron efficiency. Direct measurement of these characteristics will also help calibrate the design computer codes.

Two types of electron beam evaluation devices will be constructed and tested to experimentally verify the design of the gyrotron. The first device, a beam analyzer, will permit direct measurement of the beam geometry and velocity spread under very low duty pulsed conditions. The second device, a beam tester will evaluate the beam interception and thermal capabilities of the tube subassemblies under pulsed and cw operation with no RF interaction. Since the beam needs to be measured at full voltage and magnetic field each of these devices will use the superconducting solenoid.

#### Electron Beam Analyzer

The beam analyzer will consist of a hole scanning device which attaches directly to the electron gun and which can be slipped into the solenoid for measurement. This concept is presently used on beam analyzers for millimeter-wave Pierce guns.

The beam will be probed in the usual manner by scanning an aperture plate with a small pinhole of about 0.002 cm diameter in it across the beam and collecting the current transmitted through the pinhole in a Faraday cup. The presence of the strong magnetic field requires adequate precautions to prevent secondary electrons and reflected primaries from the collector from falsifying the results.

The beam velocity spread will be investigated by a retarding field method.

In this method a uniform axially directed retarding electric field  $E_z$  is applied in order to induce selective mirroring in the uniform magnetic field  $B_0$  of the interaction region. Figure 3.7-1 shows the apparatus schematically.

The transverse electron motion is governed by the transverse adiabatic invariant and, using previously derived equations,<sup>2</sup> one finds that

$$\frac{1}{2} \frac{m_o \gamma_s^2 v_{\perp,s}^2}{2} = \frac{1}{2} \frac{m_o \gamma_o^2 v_{\perp,o}^2}{2} = \text{const} \quad (3.7-1)$$

where the subscript s denotes the value of the variables at the collector electrode which is held at potential  $\phi_s$  and where the subscript o refers to the value of the variables before entry into the retarding field.

Since

$$\gamma = \left( \frac{e\phi}{m_o c^2} + 1 \right) = \left( \frac{\phi}{511} + 1 \right) \quad (3.7-2)$$

with  $\phi$  measured in kV one finds that since

$$v_{\perp,s} = v_{\perp,o} \frac{\left( \frac{\phi_o}{511} + 1 \right)}{\left( \frac{\phi_s}{511} + 1 \right)} = v_{\perp,o} \frac{\gamma_o}{\gamma_s} \quad (3.7-3)$$

that  $v_{\perp,s}$  is relatively unaffected by  $\phi_s$ . Changing  $\phi_s$  from 27 kV to cathode potential varies  $v_{\perp,s}$  at most by 5 percent.

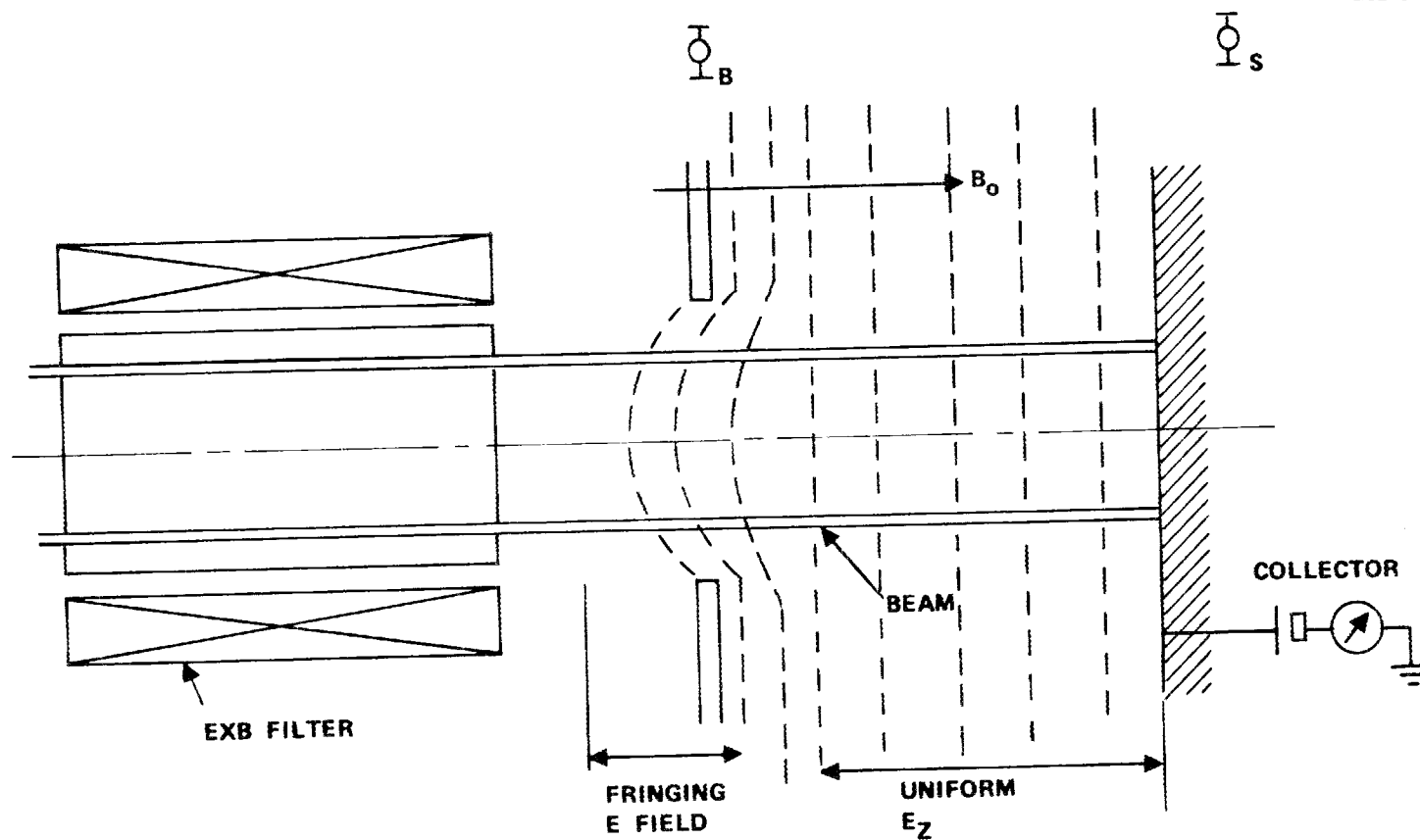


Figure 3.7-1 Proposed method of measuring axial velocity spread.

The axial velocity  $v_{z,s}$  is computed from the definition of  $\gamma$

$$1 - \frac{v_{z,s}^2}{c^2} - \frac{v_{\perp,s}^2}{c^2} = \frac{1}{\gamma_s^2} \quad (3.7-4)$$

which, on substitution for  $v_{\perp,s}^2/c^2$  from Equation (3.7-3) becomes

$$\frac{v_{z,s}^2}{c^2} = 1 - \frac{1}{\gamma_s^2} \left[ \frac{v_{\perp,o}^2}{c^2} \gamma_o^2 + 1 \right] \quad (3.7-5)$$

Substituting the tube design values into the above equation, to calculate the retarding potential of which a monoenergetic beam is reflected ( $v_{z,s} = 0$ ), we find  $\phi_s$  to be 49.45 kV.

For a transverse velocity distribution of  $\pm 2.5\%$  the electron with the largest value of  $v_{\perp}/c = 0.280$  is reflected by a voltage of  $\phi_x = 51.87$  kV. The method has therefore reasonable voltage resolution for the beam analysis.

In practice the design of the experimental equipment will be verified by computer modeling to find the perturbation produced by the fringing field of the aperture. Some concern may exist about the path of the reflected electrons which are essentially tied to the flux lines and which may produce an erroneous current reading. In Figure 3.7-1 we show a nonreciprocal element, an E-cross-B filter design to overcome this problem. Electrons heading into the collector pass through the filter undeflected, returning electrons however see a strong deflection field since the deflecting fields add for them. These electrons are collected on a suitable electrode.

### Electron Beam Tester

The beam tester will use actual gun and collector assemblies with segmented body structure which is thermally representative of the gyrotron. Each of the segments will be electrically insulated to permit direct measurement of the intercepted beam current at points along the tube. RF loss will be used along the body section to prevent oscillations from occurring. This beam tester will permit complete evaluation of the gun, magnetic focusing, and depressed collector designs under no RF conditions. The sensitivity of beam focusing to tube alignment within the superconducting solenoid will be determined. The thermal design of the gyrotron can also be verified. Following the initial experiments with the beam tester, it will be used to troubleshoot the hot test setup.

### 3.8 TEST EQUIPMENT

The unusually high operating frequency of this device, and its unique operating modes require special test equipment which will be dedicated to the program.

Commercially-available RF generators and waveguide accessories have been ordered. Measurement equipment for the 110 GHz range and for monitoring the specialized pulse modes are currently being ordered. Specialized mode converters are being designed and fabricated by Hughes.

BIBLIOGRAPHY FOR SECTION 3

1. V. K. Lygin and Sh. E. Tsimring, "Electron Trajectories in Helical Beams," Soviet Physics - Technical Physics, vol. 16, no. 11, pp. 1809-1815, May 1972.
2. J. M. Baird and K. Amboss, "90 GHz Power Tube Tecynology Study," Final Technical Report No. AFAL-TR-78-152, Sept 1978, prepared for AF Avionics Lab by Hughes Research Laboratory, Contract F33615-77-C-1240.
3. T. L. White, et al., "A Gyrotron Output Transmission Circuit," IEEE Transactions on Int Electron Devices Meeting, Dec 1978, pp. 396-398.
4. H. Jory, et al., "Development Program for a 200 kW, cW, 28 GHz Gyroklystron," Quarterly Reports Nos. 9 and 10, April-Sept 1978, prepared by Varian Associates for Oak Ridge National Laboratory under Contract No. W-7405-eng-26.
5. H. G. Unger, "Circular Waveguide Taper of Improved Design," The Bell System Technical Journal, vol. 37, July 1958, pp. 899-912.

#### IV. PROGRAM SCHEDULE AND PLANS

Attachments to this section show the work breakdown structure, milestone schedule and milestone log. Immediate plans are to continue on tasks that have already started, and to come up to speed on tasks that were originally scheduled to be underway. The hysteresis in the milestone schedule is expected to be overcome now that a formal contract has been signed (close of September 1979).

MILESTONE LOG

- Task - 1100 A Design data to power supply specs  
B Design data to beam tester, analyze  
C Design data to SN/1
- Task - 1200 A Design data to power supply specs  
B Design data to SN/2
- Task - 1300 A Design data for solenoid to beam tester, analyzer,  
Order solenoid  
B Design data for solenoid with diode gun
- Task - 1400 A Data for collector design  
B Data for SN/1 design  
C Data for SN/2 design
- Task - 1510 A Data for beam tester design  
B Data for SN/1, SN/2 design
- Task - 1520 A Data for beam tester design  
B Data for SN/1, SN/2 design
- Task - 1610 A Data for beam tester design  
B Data for SN/1, SN/2 design
- Task - 1620 A Data for beam tester design  
B Data for SN/1, SN/2 design
- Task - 1900 A Preliminary layout  
B Finalized layout

MILESTONE LOG (CONTINUED)

Task - 2110 A Magnetron injection geometry finalized

Task - 2120 A Fabrication complete

Task - 2210 A Design complete

Task - 2220 A Fabrication complete

Task - 2340 A Focus tests completed, magnetron injection gun  
B Focus tests completed, diode geometry gun

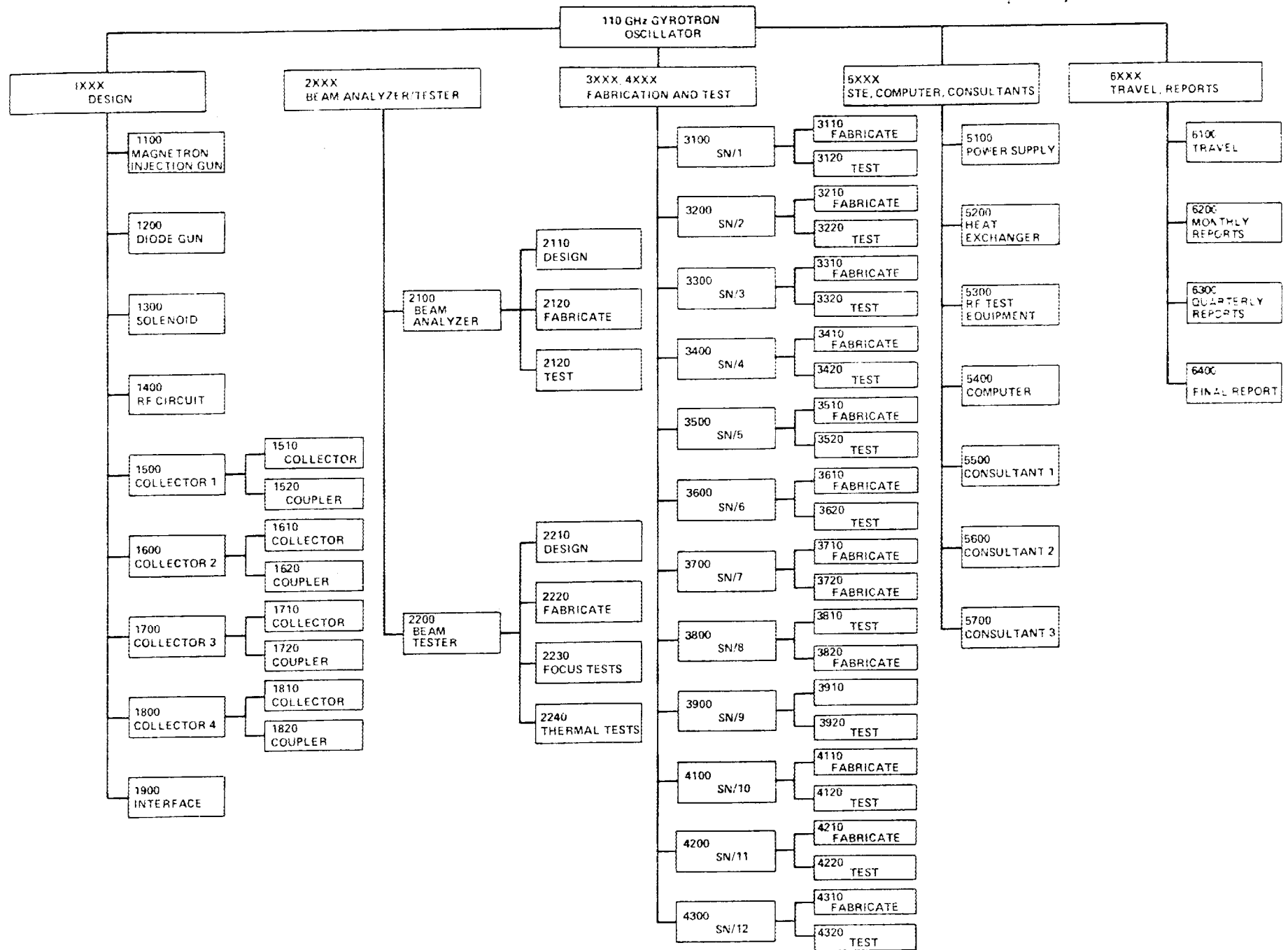
Task - 2240 A Thermal tests, collector 1  
B Thermal tests, collector 2

Task - 3110 A SN/1 assembly completed

Task - 3120 A SN/2 tests completed

Task - 3320 A SN/3 tests completed

Task - 5100 A Approved specs issued  
B Order placed  
C Manufacturers' test initiated  
D Installation at Hughes.



4-4

Figure 4-1 Work breakdown structure for 110 GHz Gyrotron - Union Carbide Corporation.

MILESTONE SCHEDULE AND STATUS REPORT - 110 GHz 200 KW GYROTRONS

HUGHES EDD, TORRANCE, CA 90509		REPORTING PERIOD 9-30-79	CONTRACT NO.	FOR UNION CARBIDE CO., OAK RIDGE, TN.	SHEET ___ OF ___																			
TASK NO.	TASK TITLE	FY 1979					FY 1980					FY 1981												
		J	J	A	S	O	N	D	J	F	M	A	M	J	J	A	S	O	N	D	J	F	M	A
1100	MAGNETRON INJECTION GUN DESIGN	██████████					██████████					██████████												
1200	DIODE GUN DESIGN	██████████					██████████					██████████												
1300	SOLENOID DESIGN	██████████					██████████					██████████												
1400	RF CIRCUIT DESIGN	██████████					██████████					██████████												
1510	COLLECTOR 1.	██████████					██████████					██████████												
1520	COUPLER 1.	○					○					○												
1610	COLLECTOR 2.	○					○					○												
1620	COUPLER 2.	○					○					○												
1900	INTERFACE/LAYOUT	○					○					○												
2110	BEAM ANALYZER DESIGN	○					○					○												
2120	BEAM ANALYZER FABRICATE	○					○					○												
2130	BEAM ANALYZER TEST	○					○					○												
2210	BEAM TESTER DESIGN	○					○					○												
2220	FABRICATE	○					○					○												
2230	FOCUS TESTS	○					○					○												
2240	THERMAL TESTS	○					○					○												
3110	FABRICATE SN/1	○					○					○												
3120	TEST SN/1	○					○					○												
3210	FABRICATE SN/2	○					○					○												
3220	TEST SN/2	○					○					○												
3310	FABRICATE SN/3	○					○					○												
3320	TEST SN/3	○					○					○												
5100	POWER SUPPLY	██████████					██████████					██████████												
5200	RF TEST EQUIPT	██████████					██████████					██████████												
6000	REPORTS MONTHLY	▼ ▼																						
	QUARTERLY																							

4-5

Figure 4-2 Milestone schedule.